

Published in final edited form as:

Nat Genet. 2020 December 01; 52(12): 1294–1302. doi:10.1038/s41588-020-00732-8.

Tissue-specific and interferon-inducible expression of non-functional ACE2 through endogenous retroelement co-option

Kevin W. Ng¹, Jan Attig¹, William Bolland¹, George R. Young², Jack Major³, Antoni G. Wrobel⁴, Steve Gamblin⁴, Andreas Wack³, George Kassiotis^{1,5,†}

¹Retroviral Immunology, The Francis Crick Institute, 1 Midland Road, London NW1 1AT, UK

²Retrovirus-Host Interactions, The Francis Crick Institute, 1 Midland Road, London NW1 1AT, UK

³Immunoregulation, The Francis Crick Institute, 1 Midland Road, London NW1 1AT, UK

⁴Structural Biology of Disease Processes, The Francis Crick Institute, 1 Midland Road, London NW1 1AT, UK

⁵Department of Medicine, Faculty of Medicine, Imperial College London W2 1PG, UK

Abstract

Angiotensin-converting enzyme 2 (ACE2) is an entry receptor for Severe Acute Respiratory Syndrome Coronavirus 2 (SARS-CoV-2) and a regulator of several physiological processes. *ACE2* has recently been proposed to be interferon-inducible, suggesting that SARS-CoV-2 may exploit this phenomenon to enhance viral spread and questioning the efficacy of interferon treatment in Coronavirus disease 2019 (COVID-19). Using a recent *de novo* transcript assembly that captured previously unannotated transcripts, we describe a novel isoform of *ACE2*, generated by co-option of intronic retroelements as promoter and alternative exon. The novel transcript, termed *MIRb-ACE2*, exhibits specific expression patterns across the aerodigestive and gastrointestinal tracts and is highly responsive to interferon stimulation. In stark contrast, canonical *ACE2* expression is unresponsive to interferon stimulation. Moreover, the *MIRb-ACE2* translation product is a truncated, unstable ACE2 form, lacking domains required for SARS-CoV-2 binding and is therefore unlikely to contribute to or enhance viral infection.

Introduction

Interferons represent the first line of defence against viruses in humans and other jawed vertebrates¹. Recognition of viral products in an infected cell results in autocrine and paracrine signalling to induce an antiviral state characterized by expression of a module of

Users may view, print, copy, and download text and data-mine the content in such documents, for the purposes of academic research, subject always to the full Conditions of use: http://www.nature.com/authors/editorial_policies/license.html#terms

[†]Correspondence: George Kassiotis, george.kassiotis@crick.ac.uk.

Contributions

K.W.N., J.A., G.R.Y. and G.K. conceived and designed the study. K.W.N., J.A., W.B., G.R.Y., J.M. and A.G.W. performed the experiments. K.W.N., J.A., W.B., G.R.Y., J.M., A.G.W. and G.K. analyzed the data. K.W.N. and G.K. wrote the manuscript with contributions from J.A., W.B., G.R.Y., J.M., A.G.W., S.G., and A.W. All authors approved the final manuscript.

Competing interests

The authors declare no competing interests.

interferon-stimulated genes (ISGs) that restrict viral replication and spread^{1,2}. Indeed, recombinant interferon is often given as first-line therapy in viral infection³ and preliminary results suggest that interferon treatment may be effective against Coronavirus disease 2019 (COVID-19)^{4,5}.

Interferon signalling results in rapid upregulation of several hundred ISGs, including genes that inhibit various stages of viral entry and replication as well as transcription factors that further potentiate the interferon response^{1,2}. Given that unchecked interferon signalling and inflammation can result in immunopathology, ISGs are subject to complex regulatory mechanisms⁶.

At the transcriptional level, long terminal repeats (LTRs), derived from endogenous retroviruses and other LTR retroelements, as well as regulatory sequences in non-LTR retroelements serve as cis-regulatory enhancers for a number of ISGs and are required for their induction⁷. Adding to this regulatory complexity, many retroelements are themselves interferon-responsive promoters and are upregulated following viral infection or in interferon-driven autoimmunity⁸⁻¹¹.

The co-evolution of viruses and hosts has resulted in a number of strategies by which viruses evade or subvert interferon responses¹². Compared with other respiratory viruses, Severe Acute Respiratory Syndrome Coronavirus 2 (SARS-CoV-2) elicits a weak interferon response despite strong induction of other chemokines¹³. Though the mechanism by which SARS-CoV-2 dampens interferon responses remains unclear, the ORF3b, ORF6, and nucleoprotein of the closely-related SARS-CoV function as interferon antagonists¹⁴. SARS-CoV-2 uses angiotensin-converting enzyme 2 (ACE2) as its primary receptor^{15,16} and recent work suggested that SARS-CoV-2 may hijack the interferon response by inducing *ACE2* expression¹⁷. By integrating multiple human, macaque, and mouse single-cell RNA-sequencing (RNA-seq) datasets, Ziegler et al. identified *ACE2* as a primate-specific ISG upregulated following viral infection or interferon treatment¹⁷. Use of an ISG as a viral receptor would result in a self-amplifying loop to increase local viral spread, and calls into question the efficacy and safety of recombinant interferon treatment in COVID-19 patients.

Using our recent *de novo* transcriptome assembly¹⁸, we identify a novel, truncated *ACE2* transcript, termed *MIRb-ACE2*, initiated at intronic *MIRb* and *LTR16A1* retroelements that serve as a cryptic promoter, alternative exon and splice site. Notably, we find that the truncated *MIRb-ACE2* and not full-length *ACE2* is the interferon-inducible isoform, and is strongly upregulated in viral infection and following interferon treatment. Importantly, the protein product of the *MIRb-ACE2* transcript does not contain the amino acid residues required for SARS-CoV-2 attachment and entry and is additionally post-translationally unstable. These findings have important implications for the understanding of *ACE2* expression and regulation, and thus for SARS-CoV-2 tropism and treatment.

Results

MIRb-ACE2* is a tissue-specific novel isoform of *ACE2

Our recent *de novo* cancer transcriptome assembly¹⁸ identified a chimeric transcript formed by splicing between annotated exons of *ACE2* and an *LTR16A1* retroelement, integrated in intron 9 of the *ACE2* locus. This transcript, which we refer to here as *MIRb-ACE2*, includes exons 10-19 of *ACE2* (Fig. 1a). Splicing between the *LTR16A1* retroelement and exon 10 of *ACE2* was highly supported by splice junction analysis of RNA-seq data from The Cancer Genome Atlas (TCGA) lung adenocarcinoma (LUAD) and lung squamous cell carcinoma (LUSC) (Fig. 1a). To identify potential transcription start site(s) of the *MIRb-ACE2* transcript, we inspected promoter-based expression analyses of the FANTOM5 data set, which indicated peaks in the *LTR16A1* retroelement and the immediately upstream *MIRb* retroelement in the same intronic region (Extended Data Fig. 1). FANTOM5 CAGE peak distribution over the *LTR16A1* and *MIRb* retroelements exhibited cell-type specificity to a certain degree, with peaks residing almost exclusively in *MIRb* in bronchial epithelial cells, but extending to *LTR16A1* in HEK293 cells (Extended Data Fig. 1). Both *LTR16A1* and *MIRb* retroelements contained multiple transcription factor binding sites, with IRF-1 and IRF-2 binding sites and TATA-box residing in *MIRb* (Extended Data Fig. 2). To further define the transcription start site(s), we performed 5' RACE (rapid amplification of cDNA ends) PCR, followed by deep sequencing of the PCR products, amplified from normal human bronchial epithelial (NHBE) cells or human squamous cell carcinoma cell lines SCC-4 and SCC-25, treated with recombinant IFN α . (Extended Data Fig. 2). Consistent with FANTOM5 CAGE data, 5' RACE analysis revealed showed multiple peaks in both *LTR16A1* and *MIRb*, again with evidence of cell-type specificity in their relative utilization (Extended Data Fig. 2). These results suggested that the *MIRb* and *LTR16A1* retroelements acted as a cryptic promoter for the *MIRb-ACE2* transcript, with transcription start sites distributed across these two retroelements.

Phylogenetic analysis of the respective *LTR16A1* and *MIRb* elements in the *Ace2* loci of representative mammalian species indicated that the ancestral integrations predated estimated dates of mammalian radial divergence (Fig. 1b). Indeed, comparative genomic analysis produced good alignment of the *LTR16A1* and *MIRb* integrations across a variety of species, with humans, dogs, and dolphins showing above 60% sequence identity to the mammalian consensus sequences of *LTR16A1* and *MIRb* (Fig. 1b, c). Of note, the *LTR16A1* and *MIRb* integrations were also present, but truncated in the murine *Ace2* locus (Fig. 1b, c), further supported by LASTz Hs-Mm whole genome alignment (Ensembl Compara databases). To further support the intronic initiation of the chimeric *MIRb-Ace2* transcript in species other than humans, we performed RT-qPCR analyses using primers complementary to the respective *LTR16A1* and *Ace2* exon 10 sequences in the African green monkey, dog, rabbit or mouse genome (Extended Data Fig. 3). Whereas all cell lines from these representative species expressed the canonical *Ace2* transcript, the *MIRb-Ace2* transcript was detected in CV-1, but not Vero cells (both from African green monkey) (Extended Data Fig. 3). The *MIRb-Ace2* transcript was undetectable in leporine R9ab and murine MCA-38 cells, but was present in canine MDCK cells (Extended Data Fig. 3), consistent with the high degree of *LTR16A1* and *MIRb* element conservation in the latter

species family. Therefore, *MIRb-ACE2* expression in humans likely represents a common mammalian feature that has been lost in some, but not all other mammalian species.

To assess the relative expression of *ACE2* and *MIRb-ACE2* isoforms, we quantified expression of both transcripts across tissue types in the TCGA and Genotype-Tissue Expression (GTEx) cohorts. Consistent with recent reports^{17,19}, full-length *ACE2* was expressed predominantly in the healthy intestine and kidney and tumors of the same histotypes (Extended Data Fig. 4). Expression of *MIRb-ACE2* followed a similar overall pattern, but with notable expression also in healthy testis, likely owing to retroelement activation as part of epigenetic reprogramming during spermatogenesis.

However, despite similar histotype distribution of *ACE2* and *MIRb-ACE2* expression, the ratio of the two isoforms was characteristically different between distinct histotypes and tumor types. For example, in larger TCGA patient cohorts, LUAD samples expressed higher levels of *ACE2* than of *MIRb-ACE2* (mean *ACE2/MIRb-ACE2* ratio = 5.63), whereas LUSC samples showed the opposite phenotype with higher expression of *MIRb-ACE2* (mean *ACE2/MIRb-ACE2* ratio = 0.87) (Fig. 2a, b). *ACE2* and *MIRb-ACE2* expression and their ratios were not affected by patient sex, arguing against a strong effect of the X chromosomal location of *ACE2* on either isoform expression (Fig. 2a, b). *ACE2* and *MIRb-ACE2* exhibited characteristic expression also within tumor types with only weak correlation between the two in the same tumor type ($R^2=0.252$ for LUAD; $R^2=0.337$ for LUSC), suggesting partly independent regulation.

In healthy lung, expression of *ACE2* and *MIRb-ACE2* was similar to that in LUAD, with the balance slightly in favor of the full-length form (mean *ACE2/MIRb-ACE2* ratio = 2.73) (Fig. 2c). By In contrast, healthy colon expressed considerably higher levels specifically of the full-length isoform (mean *ACE2/MIRb-ACE2* ratio = 26.37) (Fig. 2d). These differences in *ACE2* and *MIRb-ACE2* expression between healthy lung and colon were again independent of gender sex (Fig. 2c, d).

Tissue-specific patterns of *ACE2* and *MIRb-ACE2* expression suggested dependency on cell lineage or identity. Alternatively, they could reflect transient adaptations to the local microenvironment, such as oxygen or microbiota composition differences between lung and intestine, or even differences in cellular composition between the different compartments. To examine whether patterns of *ACE2* and *MIRb-ACE2* expression are linked to cell identity, we examined RNA-seq data from 933 cancer cell lines from The Cancer Cell Line Encyclopedia (CCLE). These represent homogenous cell populations, grown under standardized conditions, independently of environmental influences. Again, expression of *ACE2* and *MIRb-ACE2* was characteristically different between different cell lines and correlated with their anatomical origin (Fig. 3a-d). Cell lines with the highest expression of *MIRb-ACE2* were derived from the upper aerodigestive tract, including the mouth and nose (mean *ACE2/MIRb-ACE2* ratio = 0.72), followed by esophageal cells lines (mean *ACE2/MIRb-ACE2* ratio = 1.66) and lung cell lines (mean *ACE2/MIRb-ACE2* ratio = 6.27). Consistent with data from primary biopsies, cells lines from the large intestine exhibited the highest expression of *ACE2*, with minimal expression of *MIRb-ACE2* (mean *ACE2/MIRb-ACE2* ratio = 16.97). The low *ACE2/MIRb-ACE2* ratio in the upper aerodigestive tract was

highly significant when compared with other locations ($p=0.0035$, when compared with the lung; $p=0.0023$ when compared with the large intestine, Student's *t*-test).

Together, these results uncover the transcription of a novel *ACE2* isoform, initiated at the intronic *MIRb-LTR16A1* retroelements, in a characteristic pattern of expression, forming a gradient from the upper aerodigestive tract (highest *MIRb-ACE2* expression) to the large intestine (highest *ACE2* expression).

***MIRb-ACE2* and not *ACE2* transcription is IFN-responsive**

ACE2 has recently been described as a human interferon-stimulated gene (ISG), upregulated at the mRNA level following viral infection or interferon treatment^{17,20}. However, this conclusion was based mostly on analysis of single-cell RNA-seq data that might not have sufficient resolution to distinguish the two isoforms. Indeed, inspection of public single-cell RNA-seq data (GSE134355)²¹, demonstrated the limitation of such technologies, with RNA-seq reads mapping exclusively to the shared 3' terminal exon of the *ACE2* transcripts, and therefore unable to discriminate between the isoforms (Extended Data Fig. 5).

To investigate the inducibility of the two isoforms by IFN or viral infection, we re-analysed public RNA-seq data (GSE147507) from NHBE cells, treated with recombinant IFN β or infected with SARS-CoV-2, Influenza A virus (IAV) or IAV lacking the viral NS1 protein (IAV NS1)¹³. None of the treatments increased expression of full-length *ACE2* (Fig. 4a). In stark contrast, *MIRb-ACE2* expression was strongly elevated by both IAV NS1 infection and recombinant IFN β treatment, compared with mock treatment ($p=0.0005$ and $p=0.0054$, respectively, Student's *t*-test). Similar results were also obtained with analysis of lung cancer Calu-3 cells. In the absence of stimulation, Calu-3 cells express exclusively the full-length *ACE2* isoform (Fig. 4b). SARS-CoV-2 infection did not affect levels of *ACE2* expression, but noticeably induced *MIRb-ACE2* expression (Fig. 4b). Lastly, analysis of RNA-seq data from explanted lung tissue from a single COVID-19 patient demonstrated elevated expression of *MIRb-ACE2*, but not of *ACE2*, compared with healthy lung tissue (Fig. 4c), albeit statistical comparisons were not possible in this case.

To further confirm the IFN-responsiveness exclusively of *MIRb-ACE2* expression, we used SCC-4 and SCC-25 cells, which express both isoforms. Compared with mock treatment, addition of recombinant IFN α or IFN γ had a minimal effect on *ACE2* expression in SCC-4 cells and no effect in SCC-25 cells (Fig. 4d). This contrasted with very strong induction (~15-fold) of *MIRb-ACE2* expression by either type of IFN in both cell lines (Fig. 4d). Lack of *ACE* responsiveness to IFN stimulation was additionally confirmed at the protein level, where neither IFN α nor IFN γ affected levels of full-length *ACE2*, detected by Western blotting in SCC-4 and SCC-25 cells or in A549 cells, which express neither isoform and were used as a negative control (Fig. 4e). Splicing from the *LTR16A1* retroelement to exon 10 of *ACE2* is in-frame and therefore the last 449 amino acids of *ACE2* are also present in the putative *MIRb-ACE2* protein. Of note, despite strong upregulation at the mRNA level and despite using polyclonal antibodies (ab15348) targeting the C-terminus of *ACE2* present in both protein products, we were unable to detect a truncated form that would correspond to the *MIRb-ACE2* translation product in SCC-4 or SCC-25 cells (Fig. 4e).

To confirm the differential IFN inducibility of *ACE2* and *MIRb-ACE2* expression, we stimulated NHBE cells with IFN α , IFN β or IFN λ , as previously described²². Again, treatment with none of the IFNs had any measurable effect on *ACE2* expression in these primary cells (Fig. 4f). This contrasted with robust induction of *MIRb-ACE2* expression, particularly by IFN α (Fig. 4f).

Collectively, these data demonstrate that type I, II and III IFNs stimulate transcription of the *ACE2* isoform driven by the alternative *MIRb-LTR16A1*, but not the canonical *ACE2* promoter.

The MIRb-ACE2 protein product is not stable

The *MIRb-ACE2* isoform is predicted to encode a truncated *ACE2* product (amino acids 357-805) and exonization of the *LTR16A1* element creates a novel 10 amino acid N-terminal sequence (MREAGWDKGG) in the putative translation product (Extended Data Fig. 6). Importantly, this predicted protein lacks the first 356 amino acids, including the signal peptide, substrate-binding site and domains that interact with SARS-CoV and SARS-CoV-2 spike glycoproteins (Extended Data Fig. 6). Despite sharing the C-terminal half of full-length *ACE2*, which was readily detectable, endogenously produced *MIRb-ACE2* protein was not detectable in SCC-4 and SCC-25 cells naturally expressing the *MIRb-ACE2* transcript, by Western blotting using polyclonal anti-*ACE2* antibodies (ab15348) (Fig. 4e). To explore the protein-coding potential of the *MIRb-ACE2* transcript, we cloned the coding sequences of both isoforms into the pcDNA3.1 mammalian expression vector and transfected HEK293T cells, which do not endogenously express *ACE2* that would confound detection of *ACE2* produced following transfection^{16,23}. While *ACE2*-transfected HEK293T cells produced detectable full-length *ACE2*, no protein of the predicted size was detectable in *MIRb-ACE2*-transfected cells (Extended Data Fig. 7), in agreement with results using SCC-4 and SCC-25 cells (Fig. 4e). In independently reported findings²⁴, endogenously produced *MIRb-ACE2* protein could not be detected by Western blotting using the same polyclonal anti-*ACE2* serum (ab15348). However, a Myc-DDK-tagged or GFP-tagged *MIRb-ACE2* protein product was detected following overexpression in T24 cells in the same study²⁴. Moreover, a separate study²⁵ reported detection of the putative *MIRb-ACE2* protein in primary nasal epithelial cells by Western blotting using the same polyclonal anti-*ACE2* serum (ab15348), raising the possibility that the protein can indeed be translated.

To explain the apparent inefficiency of protein production from *MIRb-ACE2* transcripts, we cloned the coding sequences of both isoforms into the pcDNA3.1-DYK-P2A-GFP expression vector, which adds both a FLAG tag and P2A peptide-linked GFP as part of the protein product. Expression of GFP was comparable in *ACE2*-transfected and *MIRb-ACE2*-transfected cells, suggesting that the single RNA molecule that encodes for both the FLAG-tagged *MIRb-ACE2* product and GFP is stable and translated (Fig. 5a). Despite that, following transfection with plasmid concentrations producing readily detectable full-length *ACE2* and resulting in *MIRb-ACE2* RNA levels comparable with those endogenously produced in IFN α -stimulated cells, we could not detect the predicted *MIRb-ACE2* protein with antibodies to the FLAG tag (Fig. 5b). However, the FLAG tagged *MIRb-ACE2* protein could be detected in HEK293T cells transfected with much higher plasmid concentrations,

resulting in RNA expression levels which were one order of magnitude higher than those observed in IFN α -stimulated NHBE, SCC-4 or SCC2-25 cells (Fig. 5c). Therefore, although the *MIRb-ACE2* transcript is efficiently translated (supported by the levels of P2A-linked GFP), the MIRb-ACE2 protein product is much less abundant than the full-length ACE2 at a given RNA transcription level, suggesting post-translational protein instability of the former.

Lysine residues 625 and 702 in the full-length ACE2 protein have been described to be ubiquitinated and may contribute to its proteosomal degradation²⁶. We generated a K625R K702R (K2R) mutant of full-length ACE2, which increased protein levels, compared to the wild-type ACE2 (Fig. 5d). We have introduced the same mutations in the corresponding residues of the predicted MIRb-ACE2 protein product, K279R K356R, which were similarly accessible for ubiquitination (Extended Data Fig. 8). However, we were unable to detect stable protein following transfection with the MIRb-ACE2 K2R-encoding mutant (Fig. 5d). Consistent with this, the addition of the proteasome inhibitor MG-132 was sufficient to increase protein levels of ACE2, but did not rescue the MIRb-ACE2 protein product (Fig. 5d). Moreover, cycloheximide treatment of HEK293T cells transfected with FLAG tagged *ACE2* or *MIRb-ACE2* constructs led to the rapid loss of MIRb-ACE2 protein, but did not affect levels of full-length ACE2 in the same time frame (Fig. 5e), further supporting reduced stability of the former.

Structural considerations suggested that the MIRb-ACE2 protein product would unlikely retain the partial structure of the canonical ACE2 peptidase fold, as removing most of the this subdomain would expose the remaining component of the highly charged substrate-binding groove as well as large parts of the hydrophobic protein core (Extended Data Fig. 9). Hence, it seems unlikely that a protein coded by the *MIRb-ACE2* transcript would form a structure similar to that of the canonical ACE2. Moreover, the MIRb-ACE2 protein product lacks a canonical signal peptide and when an IgG kappa chain-derived signal peptide, which has been successfully used to express the canonical ACE2 ectodomain (residues 15-615)²⁷, was fused to the corresponding domain of the predicted MIRb-ACE2 protein (residues 1-269), there was no detectable secreted protein. These data suggest that the latter protein is subject to post-translational degradation through a proteasome-independent mechanism and therefore unlikely to exert significant biological activity.

Nevertheless, as the MIRb-ACE2 protein was indeed made under certain conditions, it remained possible that it retained some biological function or that it affected the function of canonical ACE2 through heterodimer formation. To examine this possibility, we quantified levels of enzymatically active ACE2, an assay that is considerably more sensitive than Western blotting, and found, as expected, strong enzymatic activity in lysates from *ACE2*-transfected, but not *MIRb-ACE2*-transfected cells (Fig. 5f). Furthermore, co-transfection with *MIRb-ACE2* did not affect the enzymatic activity conferred by *ACE2* transfection (Fig. 5f). To determine any involvement of the predicted MIRb-ACE2 protein in SARS-CoV-2 entry, we measured binding of the S1 subunit of SARS-CoV-2 spike glycoprotein, the first step of viral entry, to cells expressing either or both ACE2 isoforms. HEK293T cells were transfected with the P2A-GFP reporter constructs for *ACE2* and *MIRb-ACE2* and transfected and untransfected cells were distinguished based on GFP expression (Extended Data Fig. 10). Whereas SARS-CoV-2 S1 efficiently bound HEK293T cells expressing

ACE2, it did not bind those expressing *MIRb-ACE2* (Fig. 5g). Moreover, co-expression of the two isoforms in the same cells did not alter binding of SARS-CoV-2 S1, beyond the effect of plasmid dilution (Fig. 5g). Collectively, these results argue against significant effect of *MIRb-ACE2* expression on ACE2 function or SARS-CoV-2 entry.

Discussion

Regulation of ACE2 expression and function is critical both in physiology and pathology²⁸. The use of ACE2 as a primary receptor for entry by the pandemic coronaviruses, SARS-CoV and SARS-CoV-2 highlighted the potential effect of changes in ACE2 expression, particularly in response to IFN, on the course or severity of COVID-19¹⁷. Here, we show that *ACE2* transcription and protein production is not responsive to IFN. Instead, we describe a novel RNA isoform, *MIRb-ACE2*, that is highly responsive to IFN stimulation, but encodes a truncated and unstable protein product. In support of these findings, the new isoform is independently described in two other recent pre-print reports^{24,25} and matches the sequence recently deposited under GenBank accession number MT505392. We find that the *MIRb-ACE2* isoform exhibits distinct patterns of expression along the aerodigestive and gastrointestinal tracts and was likely responsible for the apparent IFN inducibility of *ACE2* expression reported by analysis of single-cell RNA-seq data¹⁷ and other similar studies²⁰. We further show that transcription of this novel isoform is initiated by intronic retroelements, which function as a cryptic, IFN-responsive promoter, adding further evidence for the widespread involvement of such retroelements in gene regulatory networks.

Indeed, endogenous retroelements comprise nearly half the human genome and can affect many host processes^{29–31}. LTR and non-LTR retroelements represent an abundant source of promoters, enhancers, and polyadenylation sequences that can modulate the expression and structure of neighboring genes³², as with *ACE2*. For instance, retroelements serve as promoters or enhancers for a number of ISGs, conferring IFN inducibility, exemplified in the case of *AIM2*⁷. Retroelements may further modify the function of ISGs and we have recently described a novel isoform of the ISG *CD274* (encoding PD-L1) that produces a truncated form through retroelement exonization³³.

The use of the intronic *MIRb* and *LTR16A1* elements as the promoter and alternative exon for the *MIRb-ACE2* isoform explains its independent regulation from that of the full-length *ACE2* isoform. In addition to IFN inducibility, the cryptic *MIRb-LTR16A1* promoter also confers tissue-specific expression, with the highest levels seen in the upper aerodigestive tract, where it can be the predominant isoform. In contrast, the canonical *ACE2* isoform far exceeds expression of the *MIRb-ACE2* isoform in the lower gastrointestinal tract. It is theoretically possible that the balance of *MIRb-ACE2* and full-length *ACE2* isoforms plays a role in the spread of SARS-CoV-2, particularly in the upper aerodigestive tract, or that RNA or protein products of *MIRb-ACE2* are involved in other pathological or physiological processes. However, the low stability of the *MIRb-ACE2* protein product argues that this is unlikely.

Independently of any functional significance, expression of the *MIRb-ACE2* isoform needs to be carefully considered in studies examining *ACE2* regulation at the transcriptional

level^{17,19,20}. The description of this novel isoform highlights the need to validate single-cell RNA-seq data with orthogonal approaches. While single-cell RNA-seq initiatives are an invaluable resource and allow for rapid identification of cell types that express a gene of interest, coverage and read depth are largely insufficient to distinguish between isoforms. Technological advances to improve sequencing depth and bioinformatic tools to impute missing values are rapidly progressing; in the meantime, long-read sequencing techniques to quantify transcript isoforms and confirmation of protein expression levels can be incorporated into existing workflows.

This work established *MIRb-ACE2* as the predominantly induced form of *ACE2* following viral infection or recombinant interferon treatment, including in the SARS-CoV-2-infected lung. The suggestion that *ACE2* is an ISG raised fears that therapeutic interferon could be detrimental¹⁷; however, we find that full-length *ACE2* is not increased at the mRNA or protein level. The predicted *MIRb-ACE2* protein product could be detected *in vitro*, albeit under high levels of *MIRb-ACE2* RNA expression, and it remains possible that the *MIRb-ACE2* protein, or fragments thereof, are produced under certain conditions *in vivo*. Indeed, despite its reduced stability when compared to full-length *ACE2*, evidence for production of the *MIRb-ACE2* protein has also been independently reported^{24,25}. Nevertheless, it is worth noting that the predicted *MIRb-ACE2* protein does not contain the residues required for SARS-CoV-2 spike glycoprotein binding¹⁵, does not bind recombinant SARS-CoV-2 S1 experimentally and is thus unlikely to contribute to viral spread. These results reconcile the apparent discrepancy between the interferon inducibility of *ACE2* with promising data showing improved outcomes in COVID-19 following interferon treatment^{4,5}.

Methods

Cell lines

HEK293T, A549, SCC-4, SCC-25, Vero, CV-1, MDCK, R9ab and MCA-38 cells were obtained from and verified as mycoplasma free by the Cell Services facility at the Francis Crick Institute. Human cell lines were additionally validated by DNA fingerprinting. HEK293T and A549 cells were grown in Iscove's Modified Dulbecco's Medium (Sigma-Aldrich) supplemented with 5% fetal bovine serum (Thermo Fisher Scientific), L-glutamine (2 mmol/L, Thermo Fisher Scientific), penicillin (100 U/mL, Thermo Fisher Scientific), and streptomycin (0.1 mg/mL, Thermo Fisher Scientific). SCC-4 and SCC-25 cells were grown in Dulbecco's Modified Eagle Medium/Nutrient Mixture F-12 (Gibco) supplemented with 10% fetal bovine serum (Thermo Fisher Scientific), L-glutamine (2 mmol/L, Thermo Fisher Scientific), penicillin (100 U/mL, Thermo Fisher Scientific), and streptomycin (0.1 mg/mL, Thermo Fisher Scientific). NHBE cells were cultured as previously described²²

Transcript identification, read mapping and quantitation

Transcripts were previously assembled on a subset of the RNA-seq data from The Cancer Genome Atlas (TCGA)¹⁸. The alternative promoter within *ACE2* was more highly expressed in lung squamous carcinomas than the canonical isoform, prompting us to investigate its biology. RNA-seq data from TCGA, GTEx, CCLE, and other studies were mapped to the cancer-tissue transcriptome assembly and counted as previously described¹⁸. Briefly,

transcripts per million (TPM) values were calculated for all transcripts in the transcript assembly¹⁸ with a custom Bash pipeline (Supplementary Code 1) using GNU parallel³⁴ v3 and Salmon³⁵ v0.12.0, which uses a probabilistic model for assigning reads aligning to multiple transcript isoforms, based on the abundance of reads unique to each isoform³⁵. Splice junctions were visualized using the Integrative Genome Viewer (IGV)³⁶ v2.4.19.

Additional bulk RNA-seq and single-cell RNA-seq data analysis

Bulk RNA-seq data were downloaded from study GSE147507¹³. Reads were adapter trimmed and filtered for minimal 35nt sequences using Trimmomatic v0.39. Since some samples were infected with SARS-CoV-2 *in vitro*, we identified and removed viral reads using BowTie2 (*seedlength* 30nt) to align reads to the Wuhan region reference genome (MN908947). Subsequently, reads were mapped with HISAT2 (optional parameters *-p 8 -q -k 5*) against GRCh38 reference chromosome assembly and transcripts were quantified against our custom transcriptome assembly using Salmon³⁵ v0.12.0, as described previously¹⁸ and above in “Transcript identification, read mapping and quantitation”.

For single-cell RNA-seq data analysis, we downloaded the raw paired end sequencing reads as unmapped bam files from study GSE134355²¹, which were already demultiplexed, with one individual per tissue per sample. We then used the *DropSeq.picard* toolbox (v2.3.0) to recapitulate processing of HCL samples as documented on ‘<https://github.com/ggjlab/HCL>’. In summary, this includes trimming polyA ends from each primary RNA sequencing read and tagging it with the cellular and molecular adapter sequence contained in the secondary read (BASE_RANGE=1-6:22-27:43-48 and BASE_RANGE=49-54, respectively). All reads were then mapped with HISAT2 (optional parameters *-p 8 -q -k 5*) against GRCh38 reference chromosome assembly. The HISAT2 index here was built with the *--exon / --ss* option to cover all known splice sites annotated in the GENCODE v34 *basic* annotation. The cellular and molecular barcode sequences were recovered using the *MergeBamAlignment* utility in *picard*.

5' RACE PCR and sequencing

Total RNA from NHBE, SCC-4 and SCC-25 cells was isolated using the QIAcube (Qiagen) and cDNA synthesis was carried out with the High Capacity Reverse Transcription Kit (Applied Biosystems), with an added RNase inhibitor (Promega). Amplicons were generated using the 5' RACE System for Rapid Amplification of cDNA Ends (Invitrogen), according to manufacturer's instructions using primers listed in Supplementary Table 1. Libraries were prepared from amplicons using the NEB Ultra II DNA Library Prep Kit for Illumina (New England Biolabs), according to manufacturer's instructions and sequenced on a MiSeq system (Illumina). Reads were quality and adapter trimmed in pairs using cutadapt³⁷ v1.18 and aligned with STAR³⁸ v2.7.1a (setting *outFilterScoreMinOverLread* = 0.1 and *outFilterMatchNminOverLread* = 0.1) to the a GRCh38 reference with known splice sites from Ensembl release 100. The most 5' base of reads mapping to the *MIRb-ACE2* transcript was taken as the TSS and were obtained from the properly-paired, uniquely-mapping reads using bedtools for visualisation within IGV v2.4.19.

MIRb and LTR16A1 sequence alignments

To identify the integration time of *LTR16A1* into the *ACE2* locus, we first compared the *Homo sapiens LTR16A1* and *MIRb* to the respective consensus sequences in Dfam³⁹. Based on sequence identity and the human neutral substitution rate estimated at 2.2×10^{-9} substitutions per site per year, the *LTR16A1* insertion is expected to be ~131 million years (with 284 nt matches across 399 nt) and the *MIRb* insertion ~155 million years (with 159 nt matches across 241 nt). To find evidence for insertion of the *LTR16A1* and *MIRb* elements before the split of the major mammalian lineages, we used the UCSC liftover utility to find the *ACE2* gene locus in Rhesus macaque (rheMac10 assembly), marmoset (caljac3 assembly), mouse (mm10 assembly), dog (canFam3 assembly), african elephant (loxAfr3 assembly), bottle-nose dolphin (Turtru2 assembly), cow (bosTau9 assembly), opossum (monDom5 assembly) and platypus (ornAna2). We used the MUSCLE aligner on default settings to build a global alignment of human to rhesus macaque and marmoset, and then aligned all other species to the profile, reverting the strand of the whole sequence for mouse, elephant, cow and opossum due to whole gene inversions. We then used muscle *-refine* on overlapping 30,000 column blocks to refine the alignment locally. Then we identified the longest potential sequences matching the *LTR16A1* and *MIRb* elements in all species based on the sequences aligning with the repeat sequence in the human genome as annotated by RepeatMasker. These were aligned to *LTR16A1* and *MIRb* consensus sequences from Dfam 3.2 with mafft (--ep 0 --genafpair --maxiterate 1000 options) and intronic sequence clearly distinct from the repeats were trimmed. The two elements are absent from the considerably shorter platypus *ACE2* intron. In opossum, the respective intronic sequence is extended but no clear matches with either *LTR16A1* or *MIRb* were found, prompting us to place both insertions ahead of the mammalian radial divergence. The illustration of the lineage tree including node times are taken from timetree.org.

Expression vectors

Open reading frames encoding *ACE2*, *MIRb-ACE2*, and respective lysine mutants were synthesized and cloned into the pcDNA3.1-DYK-P2A-GFP mammalian expression vector. Gene synthesis, cloning, and mutagenesis were performed by GenScript and verified by sequencing. Cells were transfected using GeneJuice (EMD Millipore) and harvested 48 hrs post-transfection for downstream assays.

Cell stimulation

For interferon stimulation experiments, 2×10^5 SCC-4 and SCC-25 cells were stimulated with 100 ng/mL IFN- α or IFN- γ (Abcam) or PBS for 48 hrs. For proteasome inhibition experiments, cells were cultured in 20 μ M MG-132 (EMD Millipore) 24 hrs after transfection and harvested 48 hrs after transfection. For cycloheximide experiments, cells were treated with 250 μ g/mL cycloheximide (Sigma Aldrich) and harvested at denoted time-points. NHBE cells were stimulated for 4 hrs with 1000 ng/ml IFN α , 100ng/ml IFN β or 100ng/ml IFN λ were used in a previous study²², and stored cDNA was analyzed by RT-qPCR in this study.

Western blot

Cell lysates in RIPA buffer were resuspended in SDS buffer, heat denatured at 95°C for 10 min, run on a 4-20% gel (Biorad), transferred to a PVDF membrane (Biorad), and blocked in 5% (w/v) bovine serum albumin fraction V (Sigma-Aldrich) in TBS-T. Membranes were incubated with primary antibodies to ACE2 (1:1000; ab15348, Abcam), FLAG (1:1000; F1804-50UG clone M2, Sigma-Aldrich), HRP-conjugated secondary antibodies to rabbit IgG or mouse IgG (1:1000; #7074 and #7076, respectively, Cell Signaling Technology), and HRP-conjugated actin (1:25000; ab49900, Abcam). Blots were visualized by chemiluminescence on an Amersham Imager 600 (GE Healthcare).

Reverse transcriptase-based quantitative PCR (RT-qPCR)

Total RNA from cell lines was isolated using the QIAcube (Qiagen), and cDNA synthesis was carried out with the High Capacity Reverse Transcription Kit (Applied Biosystems) with an added RNase inhibitor (Promega). Purified cDNA was used to quantify human *ACE2* and *MIRb-ACE2*, or *Ace2* and *MIRb-Ace2* in other mammalian species, using variant-specific and species-specific primers (Supplementary Table 1). The IFN-inducible human genes *CXCL10* and *CD274* were also amplified as controls for the effect of IFN treatment, using transcript-specific primers (Supplementary Table 1). For amplification of a conserved house-keeping gene, primers complementary to *HPRT* sequences conserved in all species were used (Supplementary Table 1). Values were normalized to *HPRT* expression using the C_T method.

Enzyme assays

ACE2 activity in cell lysates was measured using the SensoLyte 390 ACE2 Activity Assay (AnaSpec) according to manufacturer's instructions. Recombinant human ACE2 (Sigma-Aldrich) was used as a positive control.

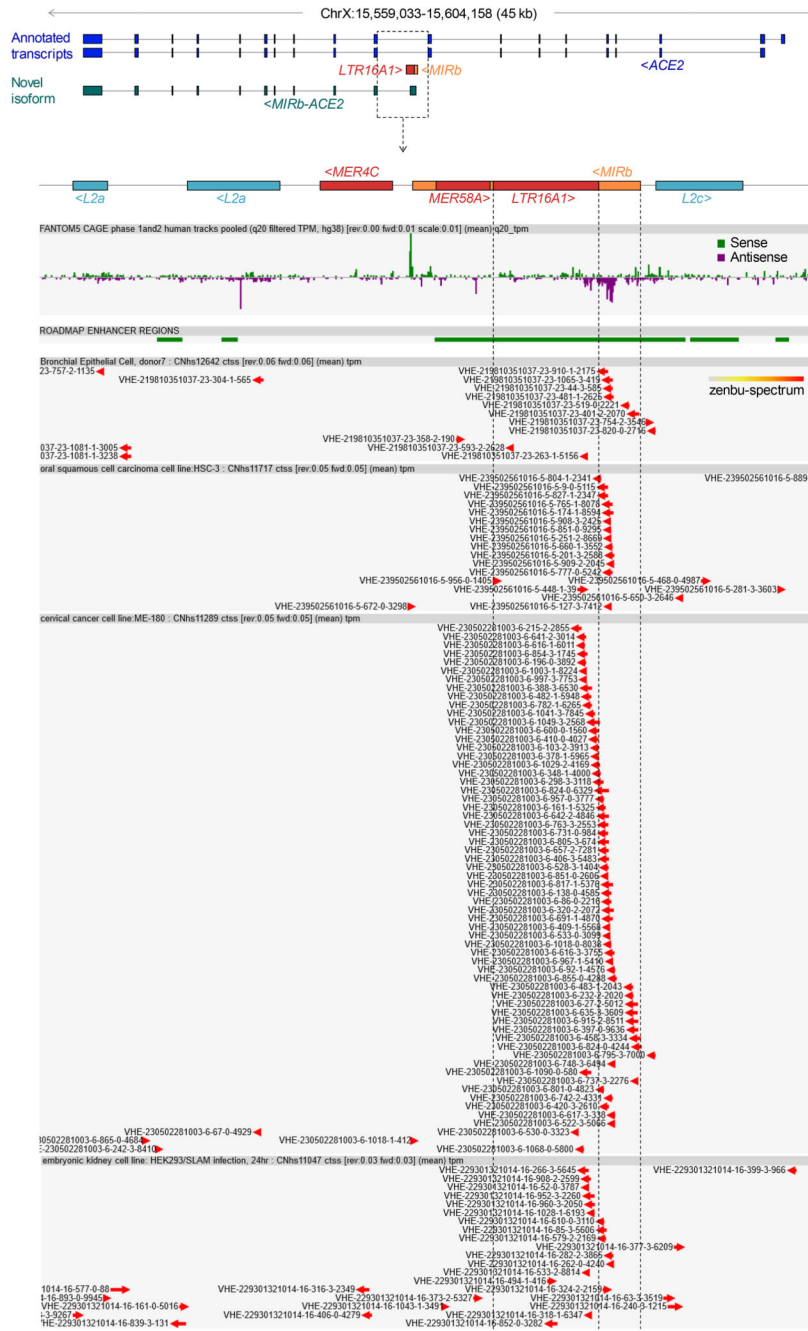
Flow Cytometry

For SARS-CoV-2 S1 binding assays, cells were stained with biotinylated S1 (1:200; Acro Biosystems) for 30 minutes followed by APC-Streptavidin (1:200; Biolegend). For S1 binding assays and for GFP detection, single-cell suspensions were run on a LSR Fortessa (BD Biosciences) running BD FACSDiva v8.0 and analysed with FlowJo v10 (Tree Star Inc.) analysis software.

Statistical analysis

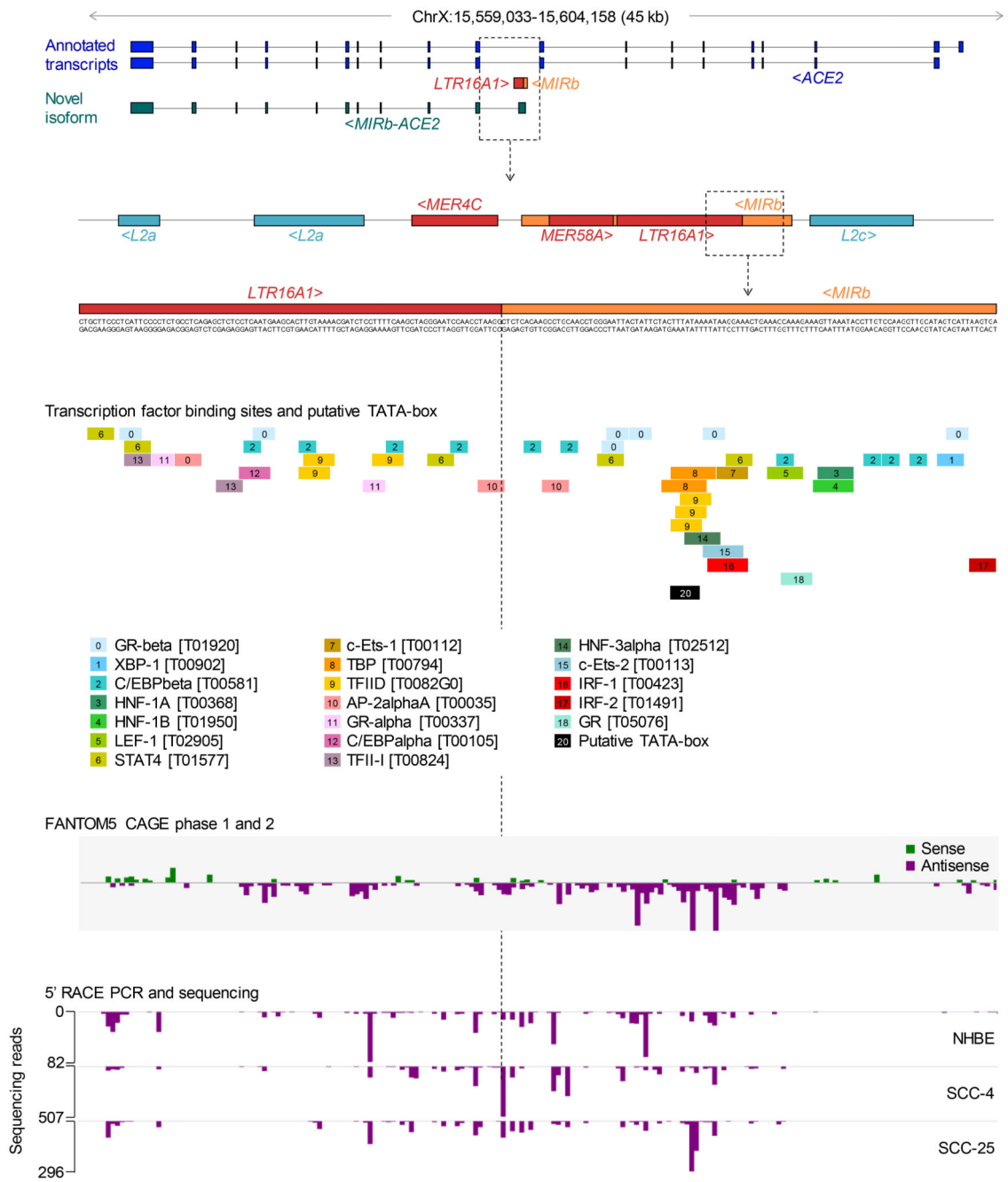
Statistical comparisons were made using GraphPad Prism 7 (GraphPad Software) or SigmaPlot 14.0. Parametric comparisons of normally distributed values that satisfied the variance criteria were made by unpaired Student's *t*-tests or One Way Analysis of variance (ANOVA) tests. Data that did not pass the variance test were compared with non-parametric two-tailed Mann-Whitney Rank Sum tests or ANOVA on Ranks tests.

Extended Data



Extended Data Fig. 1. CAGE support for transcriptional initiation of the *MIRb-ACE2* transcript
 Normalized data from the FANTOM Consortium and the RIKEN PMI and CLST (DGT) for transcription start sites in the proximity of the intronic *MIRb* and *LTR16A1* elements in the *ACE2* locus. Both the sense and antisense orientations are depicted. Data were visualized with the *zenbu* online viewer (<https://fantom.gsc.riken.jp/zenbu>) for FANTOM5 Human hg38 promoterome.

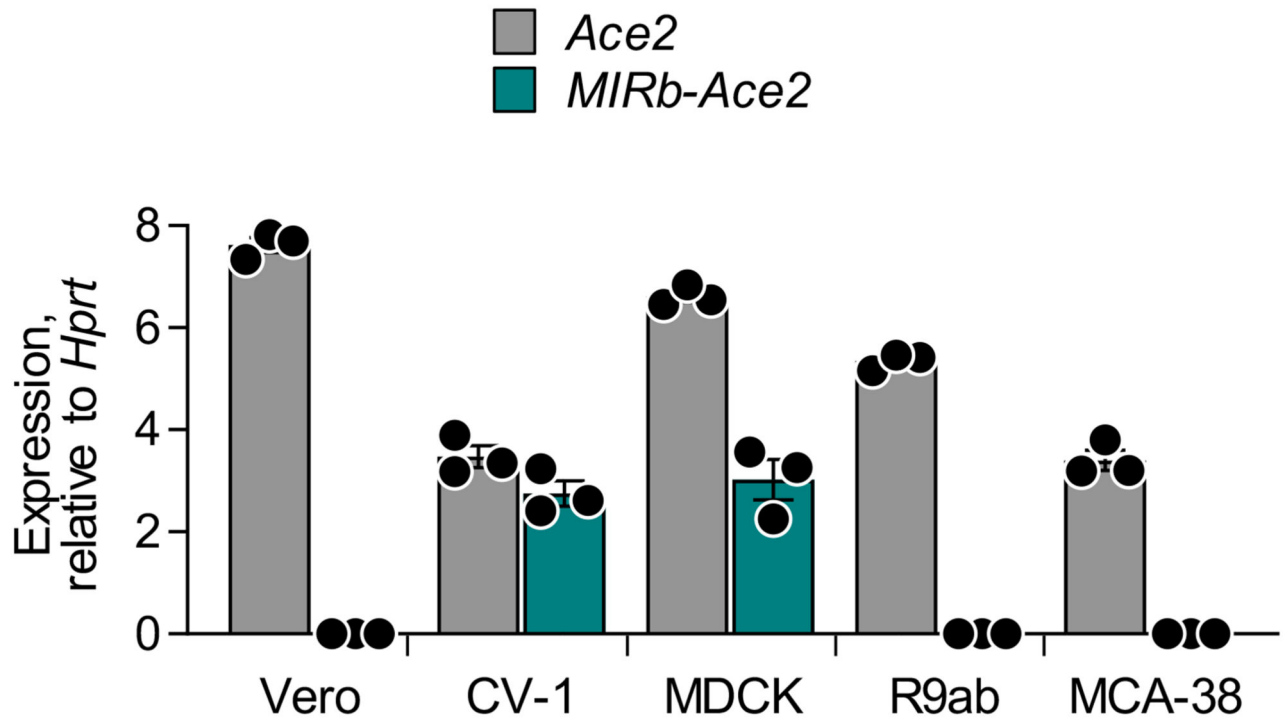
Europe PMC Funders Author Manuscripts Europe PMC Funders Author Manuscripts



Extended Data Fig. 2. 5' RACE PCR support for transcriptional initiation of the *MIRb-ACE2* transcript.

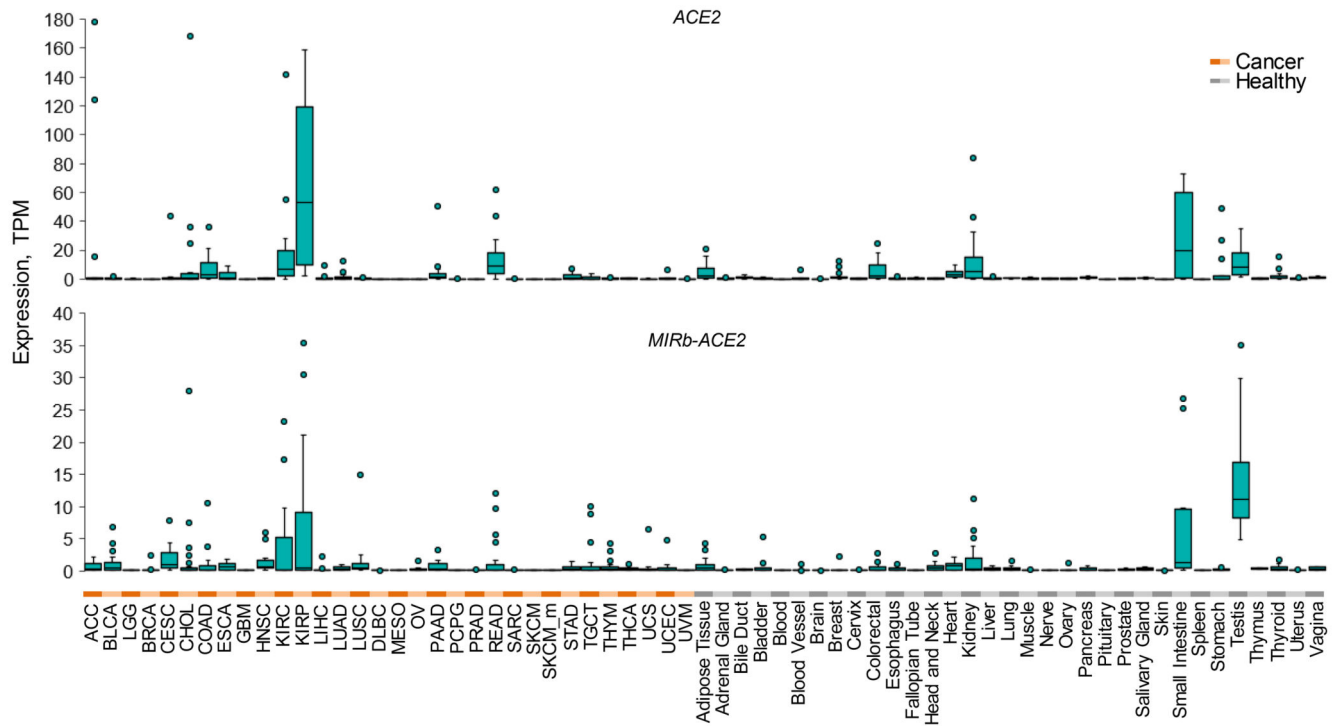
Middle panel: Putative transcription factor binding sites, predicted by PROMO (http://algggen.lsi.upc.es/cgi-bin/promo_v3/promo/promoinit.cgi?dirDB=TF_8.3), in the intronic *MIRb* and *LTR16A1* elements in the *ACE2* locus. A putative TATA-box is also depicted.

Lower panel: Mapping of sequencing reads of 5' RACE PCR products from IFN α -stimulated primary NHBE cells or SCC-4 and SCC-25 cell lines in the intronic *MIRb* and *LTR16A1* elements in the *ACE2* locus. A detailed view of CAGE data (from Extended Data Fig. 1) spanning the same region is also included for comparison.



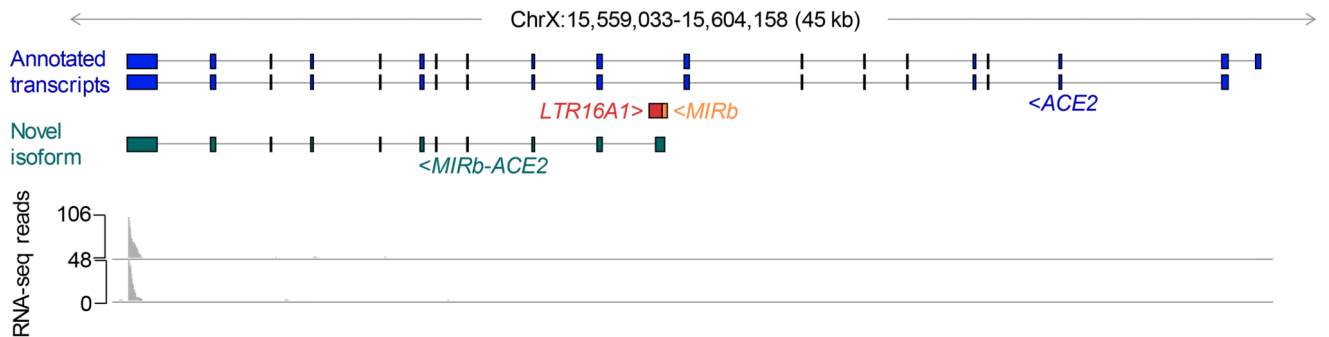
Extended Data Fig. 3. *Ace2* and *MIRb-Ace2* expression in cells from representative mammalian species.

Mean (\pm SE) *Ace2* and *MIRb-Ace2* isoform expression, determined by RT-qPCR, in Vero and CV-1 cells (both from African green monkey), and in MDCK (dog), R9ab (rabbit) and MCA-38 cells (mouse). Expression is normalized to expression of *Hprt* in each sample. Each symbol represents the mean value of two technical RT-qPCR replicates of a single culture, and the bars and error bars represent the mean and SE of the three individually-treated cultures in the same experiment.



Extended Data Fig. 4. Expression of *ACE2* and *MIRb-ACE2* isoforms in cancer and healthy tissues.

Box plots of *ACE2* and *MIRb-ACE2* isoforms expression in cancer patient and healthy control samples from TCGA and GTEx. For each cancer type, 24 samples were included (a total 768 samples), whereas for respective healthy tissues a total of 813 samples were included, varying between 2 and 156 per tissue type. Box plots show the upper and lower quartiles, center lines show the median, whiskers represent the 1.5x interquartile range and individual points represent outliers.



Extended Data Fig. 5. Single-cell RNA-seq coverage of the *ACE2* locus.

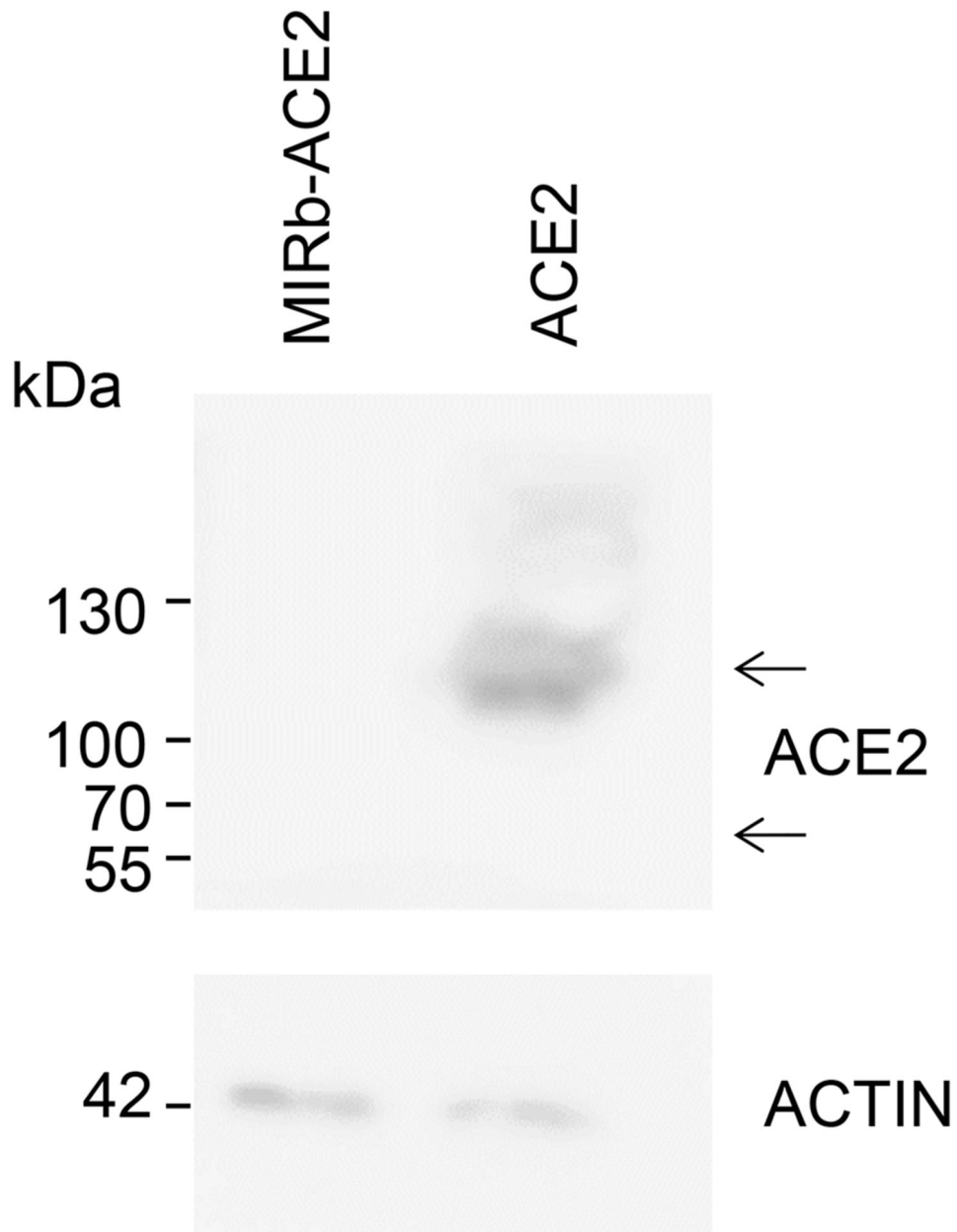
RNA-seq trace of two multiplexed samples from adult lung, obtained from study GSE134355. Note the lack of coverage across the entire locus with the exception of only the 3' end of the last exon, shared between the isoforms.

Signal peptide
 Interaction with SARS-CoV spike
 Transmembrane
 Unique sequence

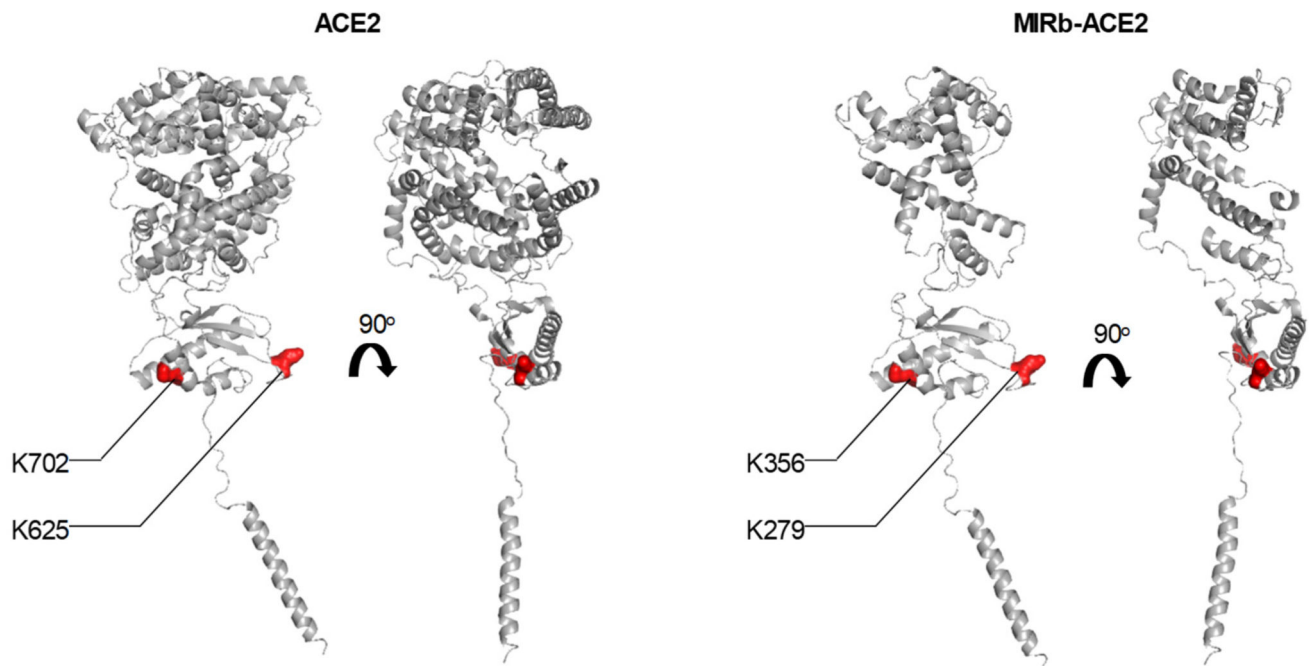
| | | | |
|-----------|-----|--|-----|
| ACE2 | 1 | MSSSSWLLLSLVAVTAAQSTIEEQAKTFLDKFNHEAEDLFYQSSLASWNYNTNI TEENVQNMNAGDKWSAFLKEQSTLAQMYPL | 85 |
| MIRb-ACE2 | | ----- | |
| ACE2 | 86 | QEIQNLTVKLQLQALQQNGSSVLSSEDKSKRLNTILNTMSTIYSTGKVCNPDNPQECLELLEPGLNEIMANSLDYNERLWAWESWRS | 170 |
| MIRb-ACE2 | | ----- | |
| ACE2 | 171 | EVGKQLRPLYEYEVVLKNEMARANHYEDYGDYWRGDYEVNGVDGYDYSRGLIEDVEHTFEEIKPLYEHLHAYVRAKLMNAYPSY | 255 |
| MIRb-ACE2 | | ----- | |
| ACE2 | 256 | ISPIGCLPAHLLGDMWGRFWTNLYSLTVPFGQKPNIDVTDAMVDQAWDAQRI FKEAEKFFVSVGLPNMTQGFWENSMLTDPGNVQ | 340 |
| MIRb-ACE2 | | ----- | |
| ACE2 | 341 | KAVCHPTAWDLGKGDFRILMCTKVTMDDFLTAHHEMGGHIQYDMAYAAQPFLLRNGANEGFHEAVGEIMSLSAATPKHLKSIGLLS | 425 |
| MIRb-ACE2 | 1 | -----MREAGWDKGRILMCTKVTMDDFLTAHHEMGGHIQYDMAYAAQPFLLRNGANEGFHEAVGEIMSLSAATPKHLKSIGLLS | 79 |
| ACE2 | 426 | PDFQEDNETEINFLKQALTI VGTLPFTYMLEKWRWVFKGEIPKDQWMKKWEMKREIVGVVEVPVPHDETYCDPASLFHVSNDY | 510 |
| MIRb-ACE2 | 80 | PDFQEDNETEINFLKQALTI VGTLPFTYMLEKWRWVFKGEIPKDQWMKKWEMKREIVGVVEVPVPHDETYCDPASLFHVSNDY | 164 |
| ACE2 | 511 | SFIRYYTRTLYQFQFQEQALCQAAKHEGPHLHKCDISNSTEAGQKLFNMLRLGKSEPWTALENVGAKNMNVRPLLNYFEPLFTWL | 595 |
| MIRb-ACE2 | 165 | SFIRYYTRTLYQFQFQEQALCQAAKHEGPHLHKCDISNSTEAGQKLFNMLRLGKSEPWTALENVGAKNMNVRPLLNYFEPLFTWL | 249 |
| ACE2 | 596 | KDQNKNSFVGWSTDWSPYADQSIKVRISLKSALGDKAYEWNDEMFLFRSSVAYAMRQYFLKVKNQMILFGEEDVRVANLKPRIS | 680 |
| MIRb-ACE2 | 250 | KDQNKNSFVGWSTDWSPYADQSIKVRISLKSALGDKAYEWNDEMFLFRSSVAYAMRQYFLKVKNQMILFGEEDVRVANLKPRIS | 334 |
| ACE2 | 681 | FNFFVTAPKNVSDII PRTEVEKAI RMSRSRINDAFRLNDNSLEFLGIQPTLGPNNQPPVSIWLVIVFGVVMGVI VVGIVILFTGI | 765 |
| MIRb-ACE2 | 335 | FNFFVTAPKNVSDII PRTEVEKAI RMSRSRINDAFRLNDNSLEFLGIQPTLGPNNQPPVSIWLVIVFGVVMGVI VVGIVILFTGI | 419 |
| ACE2 | 766 | RDRKKKNKARSGENPYASIDISKGENNPGFQNTDDVQTSF | 805 |
| MIRb-ACE2 | 420 | RDRKKKNKARSGENPYASIDISKGENNPGFQNTDDVQTSF | 459 |

Extended Data Fig. 6. Protein sequence alignment of ACE2 and MIRb-ACE2.

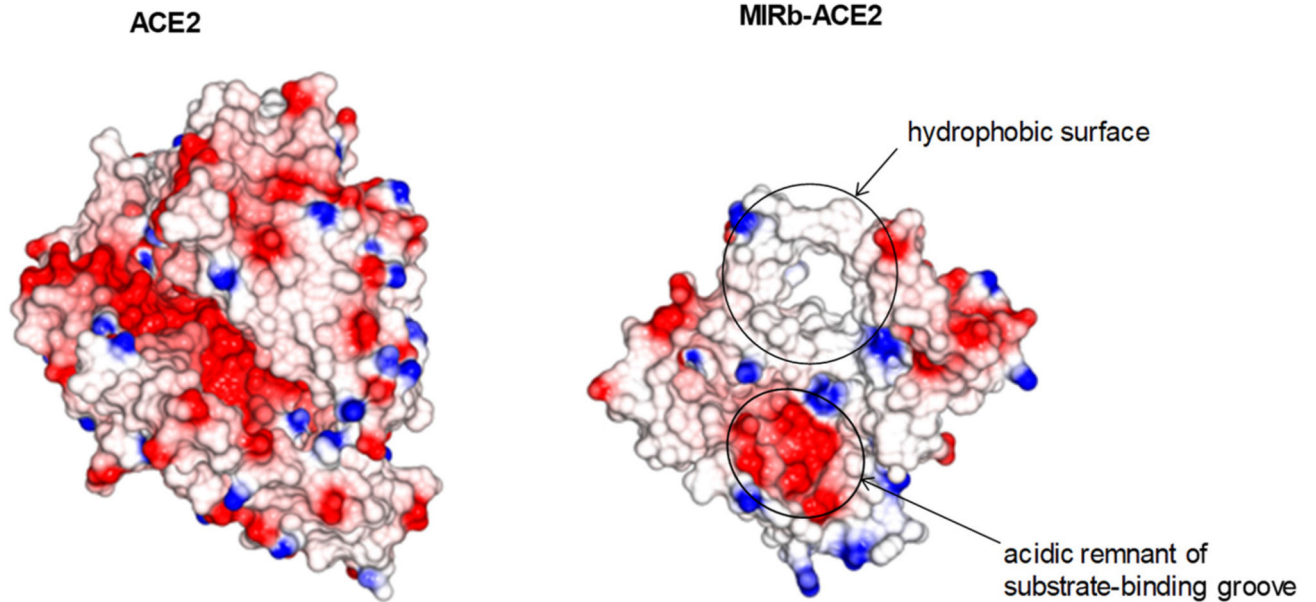
The predicted *MIRb-ACE2* translation product is a 459-amino acid protein lacking the indicated single peptide, domains interacting with SARS-CoV spike glycoprotein, but retaining the transmembrane domain. The novel 10-amino acid sequence created by *LTR16A1* exonisation is also shown.



Extended Data Fig. 7. Protein production by the *ACE2* and *MIRb-ACE2* transcript isoforms. Detection of ACE2 and putative MIRb-ACE2 protein product by Western blotting in cell lysates from HEK293T cells transfected to express either isoform. Proteins were detected using anti-ACE2 rabbit polyclonal antibodies (ab15348) as the primary reagent. One representative of 4 experiments is shown.

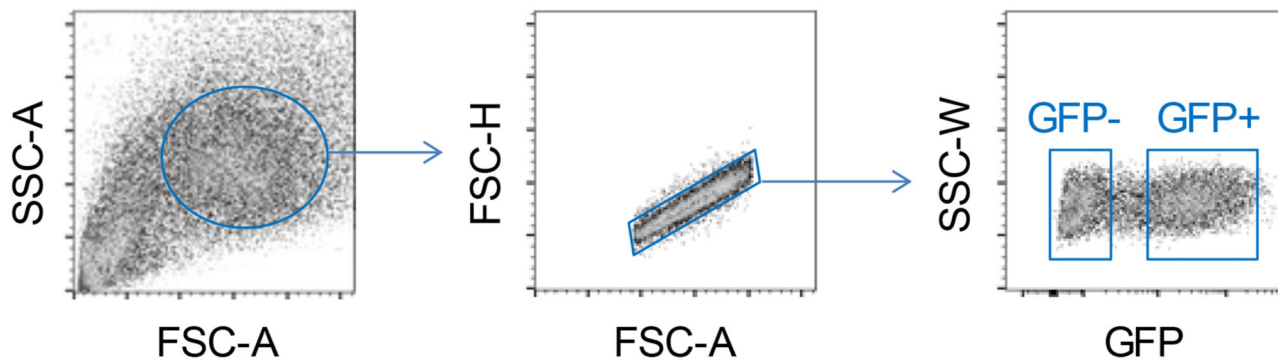


Extended Data Fig. 8. Position of the ubiquitin targets in ACE2 and MIRb-ACE2 proteins. Structure of ACE2 (*left*) and predicted structure of the MIRb-ACE2 protein product (*right*) depicting the position of the two mutated K residues, targeted for ubiquitination.



Extended Data Fig. 9. Electrostatic-surface views of ACE2 and MIRb-ACE2 proteins. Matching projections of the canonical ACE2 (PDB ID: 6M0J) and of the predicted MIRb-ACE2 protein product structures, if the latter were to exist in the same structural arrangement, but truncated. Basic, positively-charged residues shown in blue and acidic,

negatively-charged residues in red. Arrows indicate an exposed hydrophobic surface and the open, acidic remnant of the substrate-binding groove.



Extended Data Fig. 10. Identification of cells expressing *ACE2* or *MIRb-ACE2* based on GFP reporter expression.

Gating strategy for the identification of HEK293T cells transfected with plasmids encoding *ACE2* or *MIRb-ACE2* in conjunction with a P2A-GFP reporter. Expressing and non-expressing single cells were gated according to GFP expression.

Supplementary Material

Refer to Web version on PubMed Central for supplementary material.

Acknowledgments

We are grateful for assistance from the Advanced Sequencing, Scientific Computing, Flow Cytometry and Cell Services facilities at the Francis Crick Institute. The results shown here are in whole or part based upon data generated by The Cancer Genome Atlas (TCGA) Research Network (<http://cancergenome.nih.gov>). The Genotype-Tissue Expression (GTEx) Project was supported by the Common Fund of the Office of the Director of the National Institutes of Health, and by NCI, NHGRI, NHLBI, NIDA, NIMH, and NINDS. This work benefited from data assembled by the CCLE consortium. This work was supported by the Francis Crick Institute (FC001099, FC001206, FC001078), which receives its core funding from Cancer Research UK, the UK Medical Research Council, and the Wellcome Trust; and by the Wellcome Trust (102898/B/13/Z).

Data availability

Data supporting the findings of this study are available within the article and its supplementary information files. All data, plasmids and cell lines are available and from the corresponding author upon reasonable request. Publicly available data were downloaded from the following databases: The Cancer Genome Atlas (TCGA) Research Network (<http://cancergenome.nih.gov>), The Genotype-Tissue Expression (GTEx) Project (<https://gtexportal.org/home>); and the Broad Institute Cancer Cell Line Encyclopedia (CCLE) consortium (<https://portals.broadinstitute.org/ccle>). Additionally, RNA-seq data from individual studies (GSE147507 and GSE134355) were downloaded from the Gene Expression Omnibus (GEO) database (<https://www.ncbi.nlm.nih.gov/geo>). Source data are provided with this paper.

Code availability

Custom code used in this study is available in the supplementary information.

References

1. Sadler AJ, Williams BR. Interferon-inducible antiviral effectors. *Nature reviews Immunology*. 2008; 8:559–568. DOI: 10.1038/nri2314
2. Stetson DB, Medzhitov R. Type I interferons in host defense. *Immunity*. 2006; 25:373–381. DOI: 10.1016/j.immuni.2006.08.007 [PubMed: 16979569]
3. Gibbert K, Schlaak JF, Yang D, Dittmer U. IFN- α subtypes: distinct biological activities in anti-viral therapy. *British journal of pharmacology*. 2013; 168:1048–1058. DOI: 10.1111/bph.12010 [PubMed: 23072338]
4. Hung IF, et al. Triple combination of interferon beta-1b, lopinavir-ritonavir, and ribavirin in the treatment of patients admitted to hospital with COVID-19: an open-label, randomised, phase 2 trial. *Lancet (London, England)*. 2020; 395:1695–1704. DOI: 10.1016/s0140-6736(20)31042-4
5. Wang N, et al. Retrospective Multicenter Cohort Study Shows Early Interferon Therapy Is Associated with Favorable Clinical Responses in COVID-19 Patients. *Cell host & microbe*. 2020; doi: 10.1016/j.chom.2020.07.005
6. Ivashkiv LB, Donlin LT. Regulation of type I interferon responses. *Nature reviews Immunology*. 2014; 14:36–49. DOI: 10.1038/nri3581
7. Chuong EB, Elde NC, Feschotte C. Regulatory evolution of innate immunity through co-option of endogenous retroviruses. *Science (New York, N.Y.)*. 2016; 351:1083–1087. DOI: 10.1126/science.aad5497
8. Young GR, et al. Resurrection of endogenous retroviruses in antibody-deficient mice. *Nature*. 2012; 491:774–778. DOI: 10.1038/nature11599 [PubMed: 23103862]
9. Young GR, Mavrommatis B, Kassiotis G. Microarray analysis reveals global modulation of endogenous retroelement transcription by microbes. *Retrovirology*. 2014; 11:59. doi: 10.1186/1742-4690-11-59 [PubMed: 25063042]
10. Attig J, Young GR, Stoye JP, Kassiotis G. Physiological and Pathological Transcriptional Activation of Endogenous Retroelements Assessed by RNA-Sequencing of B Lymphocytes. *Frontiers in microbiology*. 2017; 8:2489. doi: 10.3389/fmicb.2017.02489 [PubMed: 29312197]
11. Tokuyama M, et al. ERVmap analysis reveals genome-wide transcription of human endogenous retroviruses. *Proceedings of the National Academy of Sciences of the United States of America*. 2018; 115:12565–12572. DOI: 10.1073/pnas.1814589115 [PubMed: 30455304]
12. García-Sastre A. Ten Strategies of Interferon Evasion by Viruses. *Cell host & microbe*. 2017; 22:176–184. DOI: 10.1016/j.chom.2017.07.012 [PubMed: 28799903]
13. Blanco-Melo D, et al. Imbalanced Host Response to SARS-CoV-2 Drives Development of COVID-19. *Cell*. 2020; 181:1036–1045.e1039. DOI: 10.1016/j.cell.2020.04.026 [PubMed: 32416070]
14. Kopecky-Bromberg SA, Martínez-Sobrido L, Frieman M, Baric RA, Palese P. Severe acute respiratory syndrome coronavirus open reading frame (ORF) 3b, ORF 6, and nucleocapsid proteins function as interferon antagonists. *Journal of virology*. 2007; 81:548–557. DOI: 10.1128/jvi.01782-06 [PubMed: 17108024]
15. Shang J, et al. Structural basis of receptor recognition by SARS-CoV-2. *Nature*. 2020; 581:221–224. DOI: 10.1038/s41586-020-2179-y [PubMed: 32225175]
16. Hoffmann M, et al. SARS-CoV-2 Cell Entry Depends on ACE2 and TMPRSS2 and Is Blocked by a Clinically Proven Protease Inhibitor. *Cell*. 2020; 181:271–280.e278. DOI: 10.1016/j.cell.2020.02.052 [PubMed: 32142651]
17. Ziegler CGK, et al. SARS-CoV-2 Receptor ACE2 Is an Interferon-Stimulated Gene in Human Airway Epithelial Cells and Is Detected in Specific Cell Subsets across Tissues. *Cell*. 2020; 181:1016–1035.e1019. DOI: 10.1016/j.cell.2020.04.035 [PubMed: 32413319]

18. Attig J, et al. LTR retroelement expansion of the human cancer transcriptome and immunopeptidome revealed by de novo transcript assembly. *Genome research*. 2019; 29:1578–1590. DOI: 10.1101/gr.248922.119 [PubMed: 31537638]
19. Singh M, Bansal V, Feschotte C. A single-cell RNA expression map of human coronavirus entry factors. *bioRxiv*. 2020; doi: 10.1101/2020.05.08.084806
20. Smith JC, et al. Cigarette Smoke Exposure and Inflammatory Signaling Increase the Expression of the SARS-CoV-2 Receptor ACE2 in the Respiratory Tract. *Developmental cell*. 2020; 53:514–529.e513. DOI: 10.1016/j.devcel.2020.05.012 [PubMed: 32425701]
21. Han X, et al. Construction of a human cell landscape at single-cell level. *Nature*. 2020; 581:303–309. DOI: 10.1038/s41586-020-2157-4 [PubMed: 32214235]
22. Major J, et al. Type I and III interferons disrupt lung epithelial repair during recovery from viral infection. *Science (New York, N.Y.)*. 2020; doi: 10.1126/science.abc2061
23. Ng KW, et al. Pre-existing and de novo humoral immunity to SARS-CoV-2 in humans. *bioRxiv*. 2020; doi: 10.1101/2020.05.14.095414
24. Onabajo OO, et al. Interferons and viruses induce a novel primate-specific isoform dACE2 and not the SARS-CoV-2 receptor ACE2. *bioRxiv*. 2020; doi: 10.1101/2020.07.19.210955
25. Blume C, et al. A novel isoform of ACE2 is expressed in human nasal and bronchial respiratory epithelia and is upregulated in response to RNA respiratory virus infection. *bioRxiv*. 2020; doi: 10.1101/2020.07.31.230870
26. Stukalov A, et al. Multi-level proteomics reveals host-perturbation strategies of SARS-CoV-2 and SARS-CoV. *bioRxiv*. 2020; doi: 10.1101/2020.06.17.156455
27. Wrobel AG, et al. SARS-CoV-2 and bat RaTG13 spike glycoprotein structures inform on virus evolution and furin-cleavage effects. *Nature structural & molecular biology*. 2020; doi: 10.1038/s41594-020-0468-7
28. Hamming I, et al. The emerging role of ACE2 in physiology and disease. *The Journal of pathology*. 2007; 212:1–11. DOI: 10.1002/path.2162 [PubMed: 17464936]
29. Burns KH, Boeke JD. Human transposon tectonics. *Cell*. 2012; 149:740–752. [PubMed: 22579280]
30. Feschotte C, Gilbert C. Endogenous viruses: insights into viral evolution and impact on host biology. *Nat Rev Genet*. 2012; 13:283–296. [PubMed: 22421730]
31. Kassiotis G, Stoye JP. Immune responses to endogenous retroelements: taking the bad with the good. *Nat Rev Immunol*. 2016; 16:207–219. DOI: 10.1038/nri.2016.27 [PubMed: 27026073]
32. Thompson PJ, Macfarlan TS, Lorincz MC. Long Terminal Repeats: From Parasitic Elements to Building Blocks of the Transcriptional Regulatory Repertoire. *Molecular cell*. 2016; 62:766–776. DOI: 10.1016/j.molcel.2016.03.029 [PubMed: 27259207]
33. Ng KW, et al. Soluble PD-L1 generated by endogenous retroelement exaptation is a receptor antagonist. *eLife*. 2019; 8doi: 10.7554/eLife.50256
34. Tange O. GNU Parallel: The Command-Line Power Tool. *The USENIX Magazine*. 2011; 36:42–47.
35. Patro R, Duggal G, Love MI, Irizarry RA, Kingsford C. Salmon provides fast and bias-aware quantification of transcript expression. *Nature methods*. 2017; 14:417–419. DOI: 10.1038/nmeth.4197 [PubMed: 28263959]
36. Thorvaldsdóttir H, Robinson JT, Mesirov JP. Integrative Genomics Viewer (IGV): high-performance genomics data visualization and exploration. *Briefings in bioinformatics*. 2013; 14:178–192. DOI: 10.1093/bib/bbs017 [PubMed: 22517427]
37. Marcel M. Cutadapt removes adapter sequences from high-throughput sequencing reads. *EMBnetjournal*. 2011; 17:3.doi: 10.14806/ej.17.1.200
38. Dobin A, et al. STAR: ultrafast universal RNA-seq aligner. *Bioinformatics (Oxford, England)*. 2013; 29:15–21. DOI: 10.1093/bioinformatics/bts635
39. Hubley R, et al. The Dfam database of repetitive DNA families. *Nucleic acids research*. 2016; 44:D81–89. DOI: 10.1093/nar/gkv1272 [PubMed: 26612867]

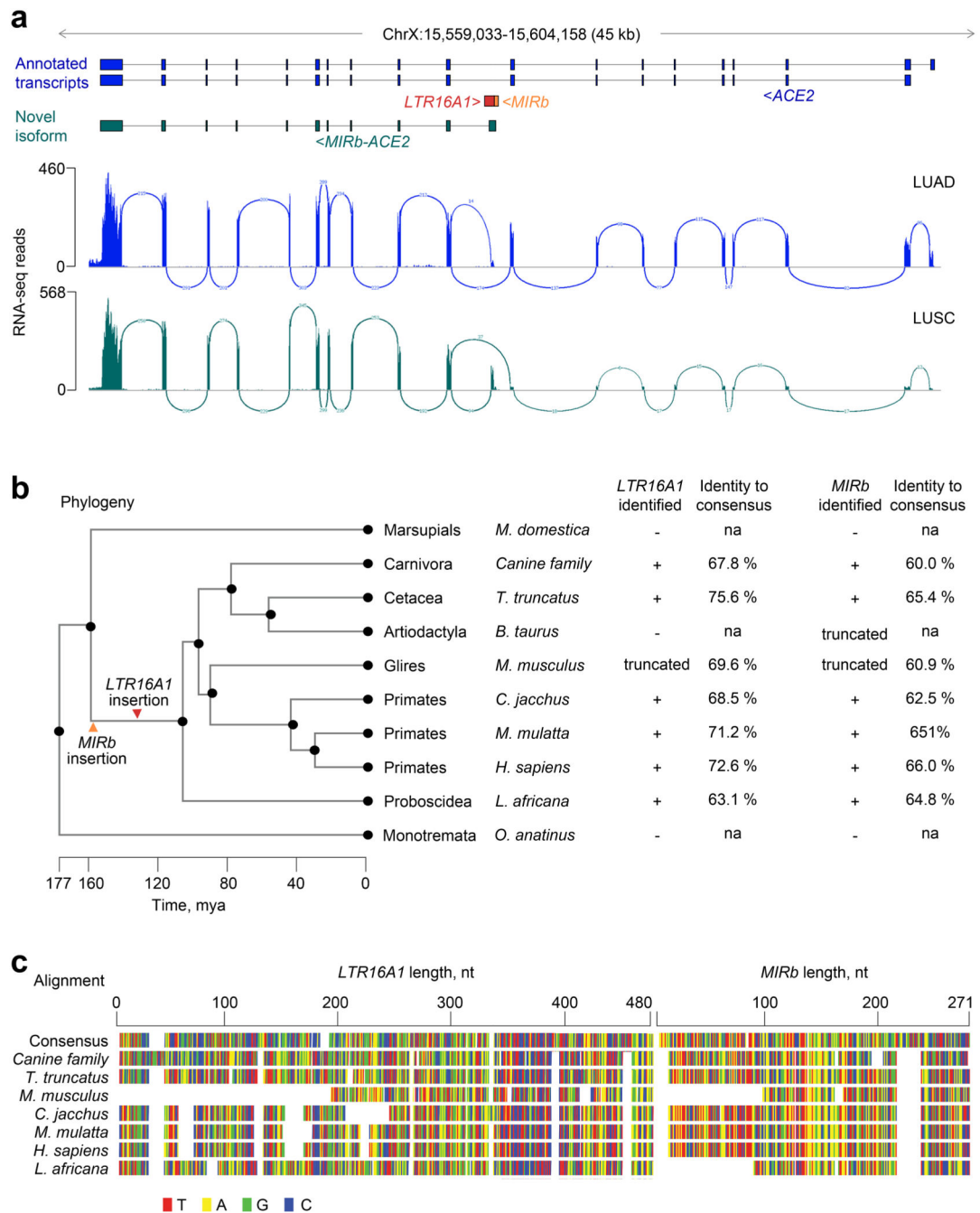


Fig. 1. Identification of the novel *MIRb-ACE2* isoform.

a. GENCODE annotated transcripts at the *ACE2* locus, intronic position of the *MIRb* and *LTR16A1* elements, structure of the novel *MIRb-ACE2* isoform and RNA-seq traces of composite LUAD and LUSC samples. Also shown is splice junction analysis of the same RNA-seq samples. **b.** Phylogenetic analysis of the *MIRb* and *LTR16A1* sequences in the indicated representative mammalian species and percent sequence identity to the consensus *MIRb* and *LTR16A1* sequences. The arrows indicate the estimated timing of ancestral integrations of the *MIRb* and *LTR16A1* elements, respectively. mya, million years ago. **c.**

Alignment of the *MIRb* and *LTR16A1* sequences in the indicated representative mammalian species and of the consensus *MIRb* and *LTR16A1* sequences.

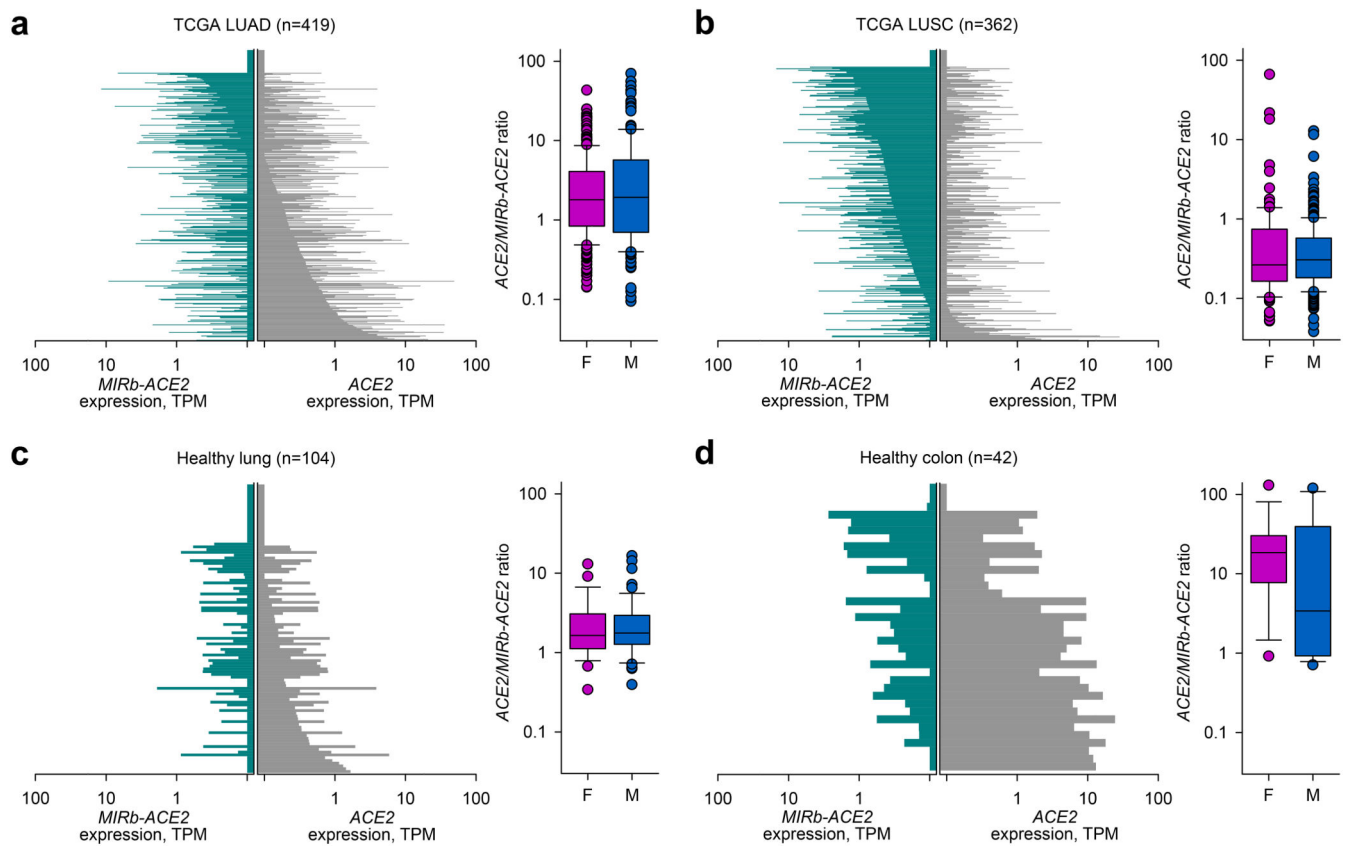


Fig. 2. *ACE2* and *MIRb-ACE2* isoform expression in cancer and healthy tissues.

a. *ACE2* and *MIRb-ACE2* isoform expression in LUAD samples (*left*) and ratio of the two isoforms in female (F, n=225) and male (M, n=161) samples (*right*). **b.** *ACE2* and *MIRb-ACE2* isoform expression in LUSC samples (*left*) and ratio of the two isoforms in female (F, n=100) and male (M, n=241) samples (*right*). **c.** *ACE2* and *MIRb-ACE2* isoform expression in healthy lung samples (*left*) and ratio of the two isoforms in female (F, n=29) and male (M, n=54) samples (*right*). **d.** *ACE2* and *MIRb-ACE2* isoform expression in healthy colon samples (*left*) and ratio of the two isoforms in female (F, n=18) and male (M, n=16) samples (*right*). In a to d, each bar represents an individual sample. Box plots show the upper and lower quartiles, center lines show the median, whiskers represent the 1.5x interquartile range and individual points represent outliers. TPM, transcripts per million

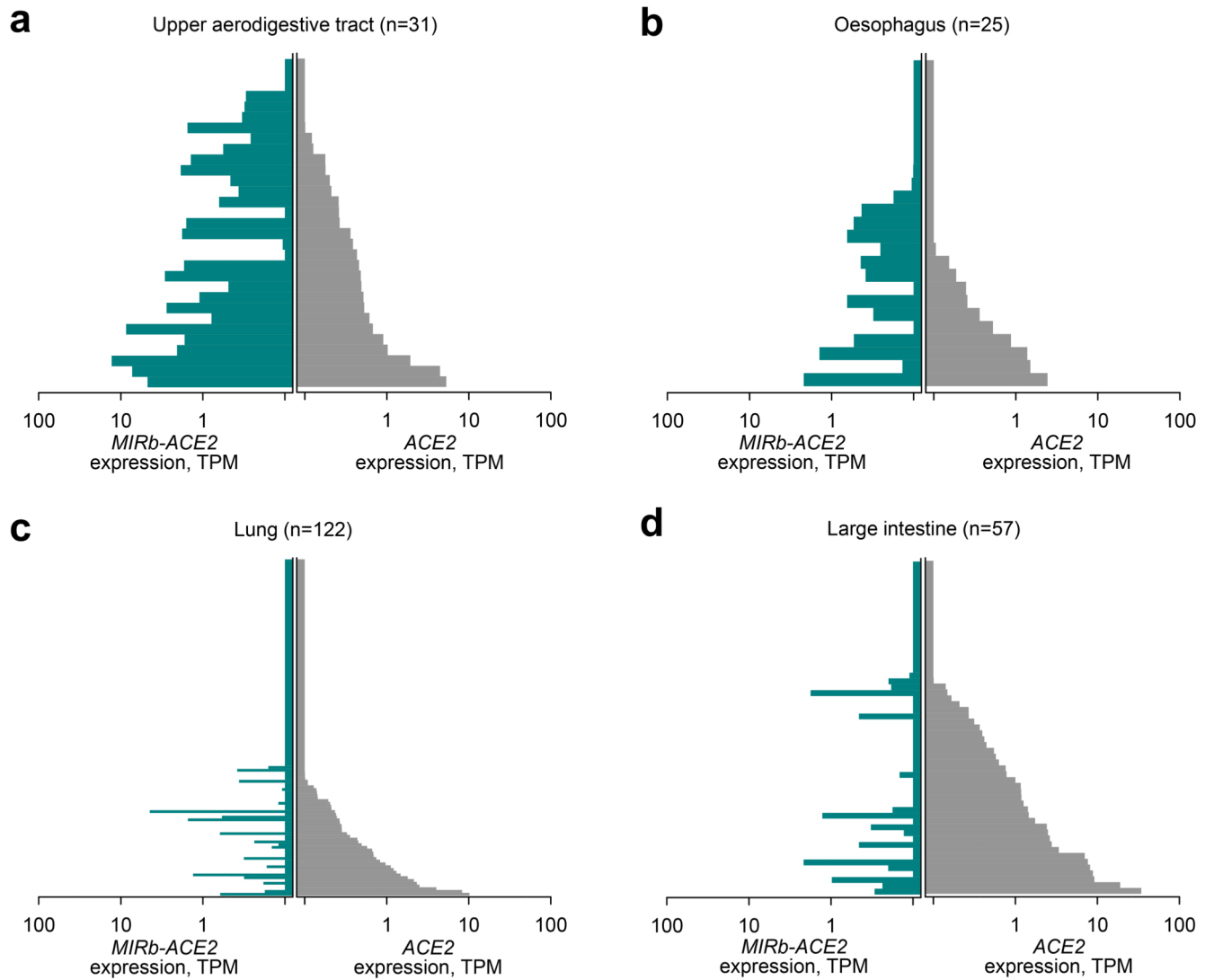


Fig. 3. *ACE2* and *MIRb-ACE2* isoform expression in cell lines.

a. *ACE2* and *MIRb-ACE2* isoform expression in cell lines from the upper aerodigestive tract. **b.** *ACE2* and *MIRb-ACE2* isoform expression in cell lines from the esophagus. **c.** *ACE2* and *MIRb-ACE2* isoform expression in cell lines from the lung. **d.** *ACE2* and *MIRb-ACE2* isoform expression in cell lines from the large intestine tract. In a to d, each bar represents an individual sample. TPM, transcripts per million.

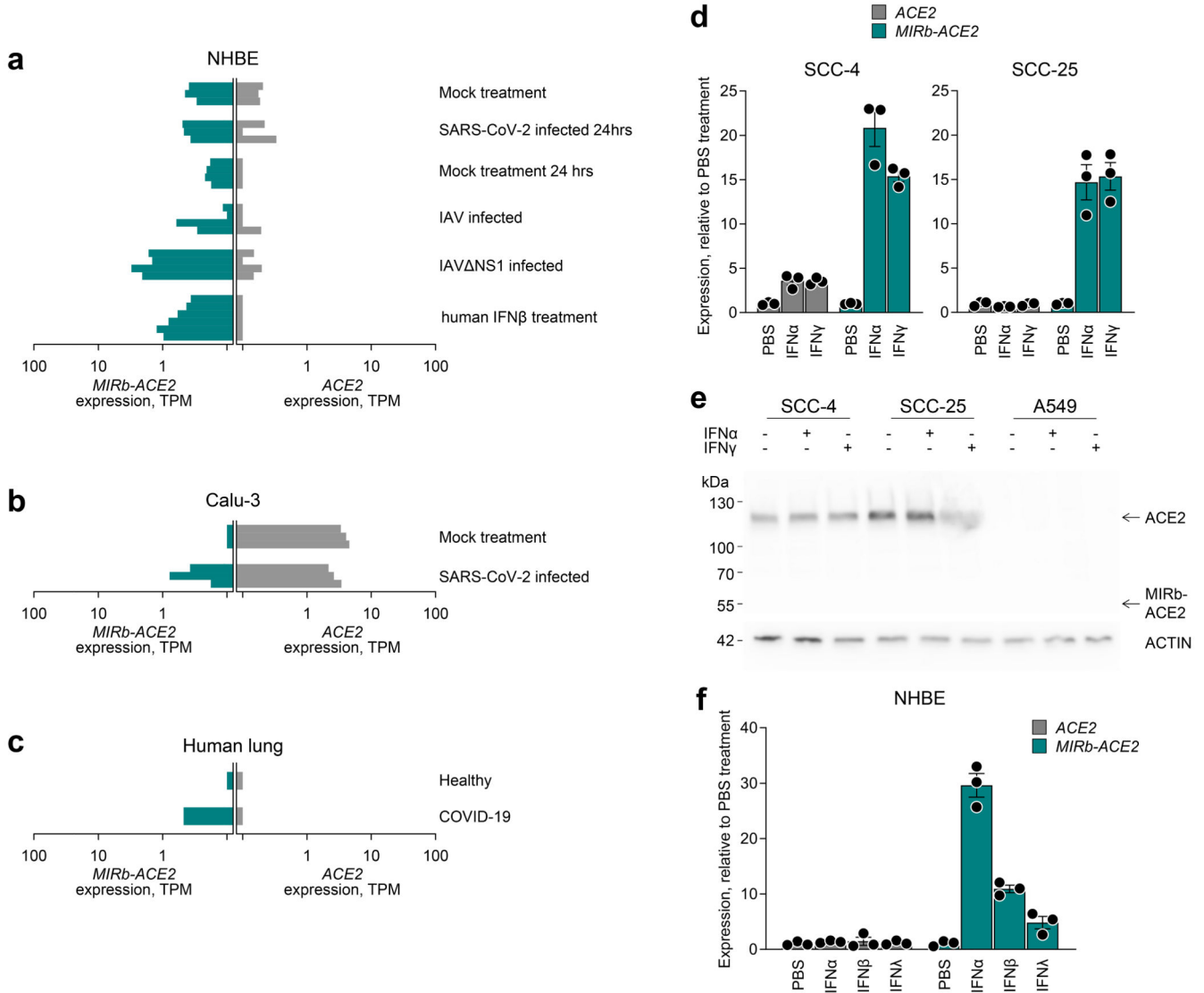


Fig. 4. IFN inducibility of ACE2 and MIRb-ACE2 isoform expression.

a, ACE2 and MIRb-ACE2 isoform expression NHBE cells following the indicated treatment. **b**, ACE2 and MIRb-ACE2 isoform expression Calu-3 cells with or without infection with SARS-CoV-2. **c**, ACE2 and MIRb-ACE2 isoform expression in the lung of a COVID-19 patient and in a healthy lung. In a to c, raw data were obtained from study GSE147507 and each bar represents an individual sample. **d**, Mean (\pm SE) ACE2 and MIRb-ACE2 isoform expression, determined by RT-qPCR in SCC-4 and SCC-25 cells with or without IFN stimulation. **e**, Detection of ACE2 and putative MIRb-ACE2 protein product by Western blotting in cell lysates from the same cells as in d. One representative of 2 experiments is shown. **f**, Mean (\pm SE) ACE2 and MIRb-ACE2 isoform expression, determined by RT-qPCR in NHBE cells with or without IFN stimulation. In d and f, each symbol represents the mean value of two technical RT-qPCR replicates of a single culture, and the bars and error bars represent the mean and SE of the three independently-treated cultures in the same experiment. TPM, transcripts per million

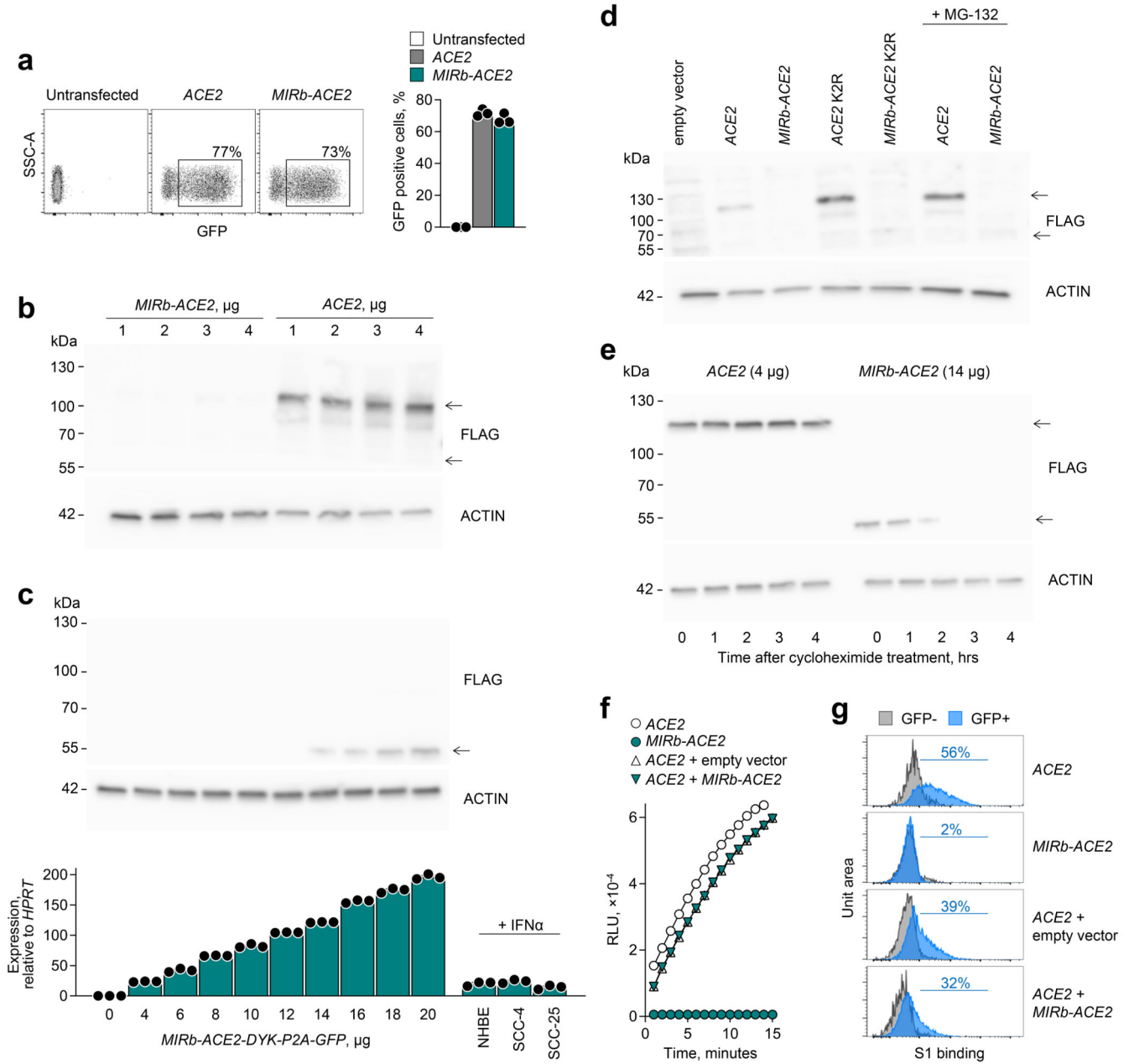


Fig. 5. Stability of the ACE2 and MIRb-ACE2 translation products.

a, Flow cytometric detection of GFP expression (*left*) and quantitation of mean frequency (\pm SE) of GFP-expressing cells (*right*) in HEK293T cells transfected to express either ACE2 or MIRb-ACE2 in conjunction with a FLAG tag and GFP, linked by a P2A peptide. Symbols represent three independently-transfected cultures in the same experiment. One representative of 3 experiments is shown. **b**, Detection of ACE2 and putative MIRb-ACE2 protein by Western blotting for the FLAG tag in cell lysates from the same cells as in **a**. Titration the transfection plasmids used is also indicated. One representative of 2 experiments is shown. **c**, Detection of MIRb-ACE2 protein by Western blotting for the FLAG tag in HEK293T cells transfected with increasing amounts of the expression plasmid

(*top*), and mean (\pm SE) *MIRb-ACE2* expression, determined by RT-qPCR in the same cells, in comparison with *MIRb-ACE2* expression in IFN α -stimulated NHBE, SCC-4 and SCC-25 cells (*bottom*). Each symbol represents the mean value of two technical RT-qPCR replicates of a single culture, and the bars and error bars represent the mean and SE of the three independently-treated cultures in the same experiment. **d**, Detection of ACE2 and MIRb-ACE2 protein by Western blotting for the FLAG tag in cell lysates from HEK293T cells transfected (with 4 μ g of expression plasmids) to express either wild-type isoform or either isoform with the two lysine residues mutated (K2R) (all in conjunction with a FLAG tag and GFP, linked by a P2A peptide). HEK293T cells transfected to express the wild-type isoforms were treated with the MG-132 inhibitor. One representative of 2 experiments is shown. **e**, Stability of ACE2 and MIRb-ACE2 protein, determined by Western blotting in HEK293T cells transfected to express either isoform, after the indicated times following treatment with cycloheximide. Data from a single experiment are shown. **f**, Kinetics of mean (\pm SD) ACE2 enzymatic activity in the supernatant of HEK293T cells transfected to express either *ACE2* or *MIRb-ACE2* or both (*ACE2 + MIRb-ACE2*). Expression plasmids were used at 4 μ g and 2 μ g each for individual transfections and co-transfections, respectively. Symbols represent the mean value of two technical replicates in the same experiment. One representative of 2 experiments is shown. **g**, Flow cytometric detection of SARS-CoV-2 S1 bindings to HEK293T cells transfected to express either *ACE2* or *MIRb-ACE2* or both (*ACE2 + MIRb-ACE2*). *ACE2* and *MIRb-ACE2* expression plasmids were used at 4 μ g and 14 μ g for individual transfections, respectively, and at 2 μ g and 14 μ g and co-transfections, respectively.